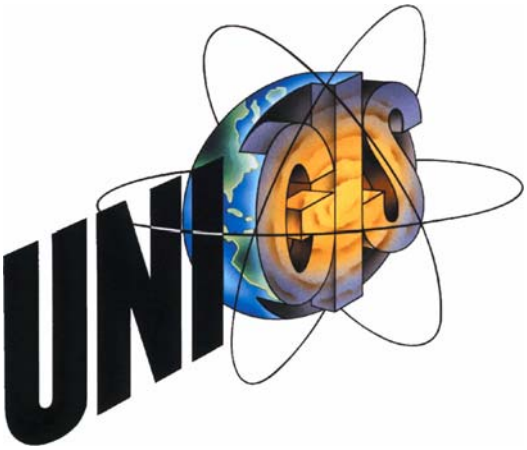

Master Thesis

within the framework of
the postgraduate studies „Geographical Information Science & Systems“
(UNIGIS MSc)
at the Centre for GeoInformatics (Z_GIS)
at the Paris Lodron University of Salzburg

GIS based coal fire risk modelling.
(Coal fire risk based on multiple geophysical and remote sensing derived data using GIS.)
A case study from Inner Mongolia Autonomous Region, China

by

Dipl.-Geoökologe Arne Bergau
U1108, UNIGIS MSc 2004

To obtain the academic title
„Master of Science (Geographical Information Science & Systems) – MSc(GIS)”

Oberpfaffenhofen, April 2006

Declaration / Erklärung

I assure that the present master thesis was carried out without external help and without using further than the stated sources. I also confirm that this thesis was not submitted to another examination board. All quotations are marked adequately.

Ich versichere, diese Master Thesis ohne fremde Hilfe und ohne Verwendung anderer als der angeführten Quellen angefertigt zu haben, und dass die Arbeit in gleicher oder ähnlicher Form noch keiner anderen Prüfungsbehörde vorgelegen hat. Alle Ausführungen der Arbeit, die wörtlich oder sinngemäß übernommen wurden, sind entsprechend gekennzeichnet.

Oberpfaffenhofen, den 10. 04. 2006

Arne Bergau

Acknowledgement

This thesis would not be existing in its current form without the help of others. Now the work is done, its time to give these persons to whom I owe my deepest thanks a thought:

- Dr. Stefan Voigt (German Remote Sensing Data Center) for including me in the ongoing project activities.
- Dr. Andreas Hirner (German Remote Sensing Data Center) for sharing his expert knowledge on local conditions in the study area and his first aid in programming tasks. Moreover for his invaluable comments on my work.
- Dr. Claudia Künzer (German Remote Sensing Data Center) for providing field data on the study area and brilliant ideas.
- Wouter Dorigo (German Remote Sensing Data Center) for his ingenious thoughts on my work and for successfully diverting me to more important things (e.g. the Kaçkar / Anatolia) in the final stage of the thesis.
- To Stefan Wessling (Leibnitz Institute for Applied Geoscience, GGA), Dr. Martin Schmidt (Federal Institute for Materials Research and Testing, BAM), Gerlinde Zybell (TU Bergakademie Freiberg), Dr. Gerlinde Schaumann (Federal Institute for Geosciences and Resources (BGR) and Tom Litschke (German Mining Technology, DMT) for willingly giving me insight in their latest research results.

Summary

Uncontrolled coal seam fires occur in all major coal producing countries world wide. Apart from causing considerate economic loss, they constitute multiple environmental hazards ranging from local to global scale. China, one of the most affected countries has an estimated annual loss of 20 - 30 Mio tons of coal per year. The associated CO_2 emissions contribute up to 0.2 % to the worldwide anthropogenic release of this green house gas.

Ongoing research activities on coal fires in the Wuda Coal Field in Inner Mongolia Autonomous Region, North Western China, incorporate remote sensing, field geological and geophysical data in development of fire detection and monitoring strategies. In this thesis, which is part of this project a framework was developed combining GIS and Dempster-Shafer Theory of Evidence to estimate fire probability based on fire indicators extracted from these data.

The employed indicators were thermal anomalies extracted from LandSat 7 satellite imagery, surface cracks and mining activity features digitized from Quickbird satellite imagery, surface temperature measurements, distribution of subsurface mining and occurrence of coal seams. Fire probability maps were generated as distance functions to the respective indicator features, the geometry of which was derived from expert knowledge. The probability maps were then combined according to Dempster's Rule of Combination to generate belief, plausibility and belief interval maps for the hypotheses „fire" and „no fire". Validation against the distribution of coal fire areas mapped in recent field investigations showed that the combined evidence from the complete data base reproduce location and extent of the known fires. Indicators were evaluated with respect to their contribution to the fire detection capability of the developed probability analysis tool. Field temperature measurements were identified to be the most important contributor followed by thermal anomalies from LandSat 7 Enhanced Thematic Mapper data. The remainder of the data was not capable of resolving single coal fire areas. For the most probable transfer scenario incorporating mainly data derived from earth observation, detectability of fires will hinge on their expression in thermal satellite imagery.

This study demonstrated that the combination of probability theory and GIS is a suitable and readily adaptable method to aggregate evidence on coal fires providing the basis for establishing priority schemes for coal fire extinguishing activities.

Zusammenfassung

Unkontrollierte Kohleflözbrände treten weltweit in allen Ländern mit bedeutender Kohleförderung auf. Sie richten dort nicht nur beträchtlichen wirtschaftlichen Schaden an, sondern stellen eine vielfältige, von lokalem bis hin zu globalem Maßstab reichende Umweltbedrohung dar. Der jährliche Verlust an förderwürdiger Kohle wird für China, das zu den am stärksten betroffenen Ländern gehört, auf 20 – 30 Mio. Tonnen beziffert. Die damit verbundenen CO_2 Emission machen bis zu 0,2 % der jährlichen anthropogenen Gesamtemissionen dieses Treibhausgases aus.

Im Rahmen aktueller Forschungsaktivitäten an Kohlebränden in der Wuda Kohlebergbauregion (Nordwest-China, Autonome Region Innere Mongolei) werden basierend auf geologischen Felduntersuchungen und Erdbeobachtungsdaten Feuererkennungs- und Überwachungsstrategien entwickelt. Gegenstand dieser Arbeit war die Integration von feuerrelevanten Indikatoren, die aus diesen Daten abgeleitet werden können, in ein GIS gestütztes Modell der Feuerwahrscheinlichkeit.

In den auf der Dempster-Shafer Theory of Evidence basierenden Ansatz wurden sechs Indikatoren einbezogen: aus LandSat 7 Daten extrahierte thermale Anomalien, von hochauflösenden Quickbird Daten abdigitalisierte Oberflächenrisse und über tage sichtbare Indizien für Bergbauaktivität, Messungen der Oberflächentemperatur, sowie die Verbreitung von Untertagebau und Kohleflözen. Für die Indikatoren wurden Feuerwahrscheinlichkeitskarten generiert, wobei die Wahrscheinlichkeit als eine Funktion der Distanz interpretiert wurde. Die Geometrie dieser Funktion wurde aus Expertenwissen abgeleitet. Die Wahrscheinlichkeitskarten wurden gemäß der Dempster Regel kombiniert um Belief, Plausibility und Belief Interval Karten für die Hypothesen „Feuer“ und „kein Feuer“ zu erstellen. Die Validierung gegen eine im Rahmen jüngster Kartierarbeiten entstandenen Brandaktivitätskarte zeigte eine gute Übereinstimmung der modellierten Feuerwahrscheinlichkeit mit Lage und Ausdehnung der bekannten Brandzonen im Untersuchungsgebiet. In einer Sensitivitätsanalyse wurden die Indikatoren mit dem größten Beitrag zur Vorhersagerichtigkeit der Methode ermittelt. Die Oberflächentemperatur Messungen erwiesen sich dabei als der Datensatz mit dem größten Einfluss, gefolgt von den thermalen Anomalien. Die übrigen Datensätze tragen nicht signifikant zur Auflösung einzelner Brandzonen bei. Im wahrscheinlichsten Transfer Szenario, das vorwiegend auf Satellitendaten beruht, wird die Detektierbarkeit

von Feuern wesentlich von ihrer Ausprägung als Anomalien in thermalen Satellitendaten abhängen.

Die vorliegende Arbeit zeigte, dass die Kombination von Wahrscheinlichkeitstheorie und GIS eine geeignete und beliebig anpassbare Methode darstellt um thematisch vielschichtige Information über Kohlefeuer zu aggregieren. Die abgeleiteten Feuerwahrscheinlichkeitskarten können als Basis für die Koordinierung von Löschaktivitäten dienen.

List of Figures

List of Tables

List of Symbols and Acronyms

°C	Degree Celsius
⊕	Orthogonal Sum
µm	Micrometer
Θ	Frame of Discernment
Ø	Empty set
Bel	Belief
BP	British Petroleum
BPA	Basic Probability Assignment
CH_4	Methane
CO	Carbonmonoxide
CO_2	Carbondioxide
COM	Component Object Model
DFD	Deutsches Fernerkundungsdatenzentrum
DLR	Deutsches Luft- und Raumfahrtzentrum
DMT	Deutsche Montan Technik
dpi	Dots per inch
DS	Dempster-Shafer
DST	Dempster – Shafer Theory of Evidence
EO	Earth Observation
ETM+	Enhanced Thematic Mapper
GIS	Geographical Information System
GPS	Global Positioning System
K	Kelvin
LS7	LandSat 7
MCE	Multicriteria Evaluation
Mio.	Million
MIR	Middle Infrared
N_2O	Nitrous Oxide
NIR	Near Infrared
NO_x	Nitrogenoxide
m	Mass of belief
Pl	Plausibility

TIR	Thermal Infrared
UTM	Universal Transverse Mercator
VB.NET	Visual Basic.NET
WGS 84	World Geodetic System 1984
yr	Year

Table of content

1. Introduction

1.1 Coal fires

Today, uncontrolled coal seam fires constitute an environmental and economic problem of global extent. They occur in coal mining areas in many countries worldwide, including China, India, Russia, the United States, Australia and at a smaller scale also in Europe (WALKER, 1999). China is among the countries most seriously affected by coal fires. The country is leading with respect to coal production, consumption and export and its energy supply is highly dependant on coal. An estimated 20 to 30 Mio tons of coal is burnt by uncontrolled coal fires each year and the tenfold amount is lost, as adjacent coal becomes inaccessible (KÜNZER, 2005). Given a market price (North Western Europe) of 70 US Dollars per ton in 2004 (BP, 2005) the economic loss sums up to 21 Billion US Dollars.

Moreover, the economic loss coal fires pose serious environmental hazards. On local scale gaseous (in particular the toxic compounds nitrogen oxides (NO_x), carbon monoxide (CO) and sulphur dioxide (SO_2)) and solid combustion products are massive contamination sources for both the air and the groundwater. Intake of toxic substances through inhalation, ingestion with agricultural crops or drinking water seriously threatens health of mine workers and residents. Moreover, subsidence caused by subsurface volume loss can be a threat to buildings and infrastructure. Last but not least several hundred mine workers are killed each year in mining accidents which are often fire related (KÜNZER, 2005).

On global scale coal fires contribute considerably to emission of the greenhouse gas nitrogen dioxide (CO_2) and, to a smaller extent, methane (CH_4) and nitrous oxide (N_2O). According to recent estimations emissions by Chinese coal fires account for 12 % of total Chinese coal based CO_2 emissions and up to 0.2 % of global annual emissions induced by burning of fossil fuels (KÜNZER ET AL, IN REVIEW).

Ignition and perpetuation of coal fires depend on the presence of the factors fuel, oxygen and energy. In the case of coal seam fires, left over coal debris and the unmined seam provide the fuel, while oxygen is supplied by the air circulating through ventilation systems and natural cracks. With respect to the energy essential for ignition of a coal seam fire, three sources are known: anthropogenic activity, natural hazards and spontaneous combustion (WALKER, 1999). Coal mining is the prime anthropogenic

ignition source and risks are especially high in less developed countries. In these countries, careless use of explosives or open fire combined with low security standards is often encountered in small private or illegal coal mines. Another cause of mine fires may be the misuse or improper maintenance of mechanical and electrical mining equipment. Major natural ignition causes are lightening strike at coal seam outcrops or forest- and bush fires. Spontaneous combustion is the most common cause for coal fires. The term refers to a chain of reactions triggered by the adsorption of oxygen at large surface of the porous medium coal. Due to the exothermic character of this reaction heat is produced. When heat production exceeds dissipation of the heat, the temperature rises and above a threshold of approximately 80 °C the process accelerates finally leading to combustion of coal (WALKER, 1999). Coal fires not only occur in coal seams but also in coal waste piles or in coal heaps. According to their causes, depth and activity status coal fires can be further distinguished (Table 1).

Table 1.1: Classification of coal fires after ZHANG (2004)

First Class	Second Class	Attributes
Coal seam fire	Natural coal fire	Surface/Underground or Subsurface
	Coal mine fire	Paleo/Recent
Coal heap fire	Coal Waste fire	Extinct, dormant, active
	Coal stockpile fire	

The enormous destructive potential of coal fires explains the urgent need to develop methodologies for detection, monitoring and extinction of fires. Coal fires in China have recently been subject to extensive research activities. Because of the large areal extent of the phenomenon and the remoteness of many coal fields, much of the work was focused on the capability of remote sensing to detect fires (VAN GENDEREN & GUAN 1997; ZHANG, X. 1998; WANG 2002; ZHANG, J. 2004; KÜNZER, 2005).

1.2 Project context

In 2003 the joint Sino German on coal fires was launched. The project "Coal Fire Research – A Sino German initiative (http://www.coalfire.caf.dlr.de/intro_en.html) (8.4.2006) is funded by the German ministry of Education and Science (BMBF) and the

Chinese Ministry of Science and Technology (MOST). The German Remote Sensing Data Center (DFD) of the German Aerospace Center (DLR) is in charge of coordinating the initiative. The project is addressing the problem of coal fires from a multidisciplinary point of view. Remote sensing, geology, geophysics, chemistry and mining technology contribute to investigations on

- detection and quantification of coal fires,
- thermo dynamical and rock mechanical modelling of fires,
- simulation of the spontaneous combustion process,
- geophysical signature of fires and
- environmental impacts of fires.

The overall goal is to provide the scientific basis and techniques allowing for development of efficient assessment, monitoring and extinction strategies for coal fires in China. Remote sensing and airborne geophysical investigation provide information on surface and depth distribution of potential subsurface combustion zones, while modelling activities promote understanding of the in situ processes. The planned extinction activities are explicitly intended to support the Kyoto Process by reducing fire induced greenhouse gas emissions. They can now be accredited in the framework of the "Clean Development Mechanism" and the reduction of gas emissions can be traded as "Certified Emission Reductions".

1.3 Aim and objectives of this thesis

One of the initial project goals was to integrate results from different research views. Up to now some steps in this direction have been undertaken in the realm of chemical, thermo dynamical and mechanical modelling. Another step is the implementation of a data warehouse at DFD, where the resulting data sets are currently being collected and managed (HIRNER, 2005 PERS. COMM.). By allowing for storage of multiple data formats and user defined querying the warehouse promotes the exchange of research results among the project partners. Yet, most data sets are still in a proto type phase and as to now no concept for an automated procedure integrating the different data formats and thematic information on fires has emerged. This procedure is to play a key role in developing fire risk assessment strategies applicable to different

coal mining areas in China. It should provide easy to use and comprehensible decision support for fire extinguishing activities. The approach developed in this thesis constitutes a GIS based framework for such an procedure. Accordingly, the goals specific to this thesis were on the conceptual level

1. to find a synthetic parameter capable to abstract fire relevant information from different data sets,
2. to find a GIS based method to model and visualize the spatial distribution of this parameter.

On the implementation level goals were

3. to find an adequate way to deal with uncertainty in the available data,
4. to investigate whether fires in the study area can be located more accurately by combining information from multiple data sets,
5. to ensure transferability of the approach to other coal fire areas.

Achievement of the latter goal could not be verified due to the lack of data for transfer regions.

The at hand thesis is structured into seven chapters. Chapter 2 contains a short description of geologic and mining related characteristics of the study area. In chapter 3 different probabilistic approaches, Fuzzy Set Theory, Bayesian Probability Theory and Dempster-Shafer Theory of Evidence (DST) are introduced to deal with uncertainty in decision making. Furthermore recent advances in theory and geo related application of probability theory with focus on DST are briefly summarized. Chapter 4 presents the data sets incorporated in this thesis. Based on general considerations concerning the decision problem associated with coal fires Chapter 5 describes the methodology to model coal fire probability. Chapter 6 introduces the software used to implement the theoretical model. In chapter 7 results for the study area are presented and expected results for different transfer scenarios are discussed. Chapter 8 contains a brief conclusion and recommendation for further research

2. Study area

Three coal fields in the northern coal mining belt in China were chosen as areas of interest within the research initiative. Among these, the Wuda area is investigated most thoroughly. Geologic and mining related data is available for the area along with abundant field data on coal fire characteristics. It was therefore selected as study area in the frame of this thesis.

2.1 Geographic location and Geology

The Wuda area includes Wuda coalfield and its surrounding areas in the Inner Mongolia Autonomous Region (figure 2.1). Wuda coalfield is located at 39°28'-39°34'North and 106°36'40''-106°38'41''East, and extends 10 km from North to South and 3-5 km from East to West, covering an area of 35 km^2. It is framed by the Yellow River in the East and the Helan mountain range in the South. Tectonically, the coalfield comprises a synclinal structure holding a total reserve of 630 Mio tons of coal. The coal originates from Permian times (GIELISCH, 2004). Of the total deposits, exploitable reserves are stated to be 27 Mio tons. Altogether 27 coal seams are found in the coalfield, 12 of which are featuring a stable distribution and are therefore mined throughout the whole field. Average thickness of these seams is 33.6 m and common dip angles range between 5 and 15 °. Coal is mined within three independent coal mining fields. From these fields three different quality types of coal - fat coal, cooking coal and steam coal - are being extracted (ZHANG, 2004).

2.2 Coal Mining

Since commercial mining started in 1958, 120 megatons had been mined by 2000. Large scale mining is mainly in the hand of the state but partially also performed by private business (ZHANG, 2004). Herein, mechanized longwall methods are applied to a maximum depth of 300 m, whereas the average depth is 100 m below ground surface level (GIELISCH, 2004). Private small scale mining is permitted since 1980. However, many of the formerly more than 100 small scale mines are now abandoned after coal

fires had made mining too dangerous. Since mine entries and ventilation systems were often sealed off improperly, these abandoned mines still constitute risk areas for spontaneous combustion of coal seams.

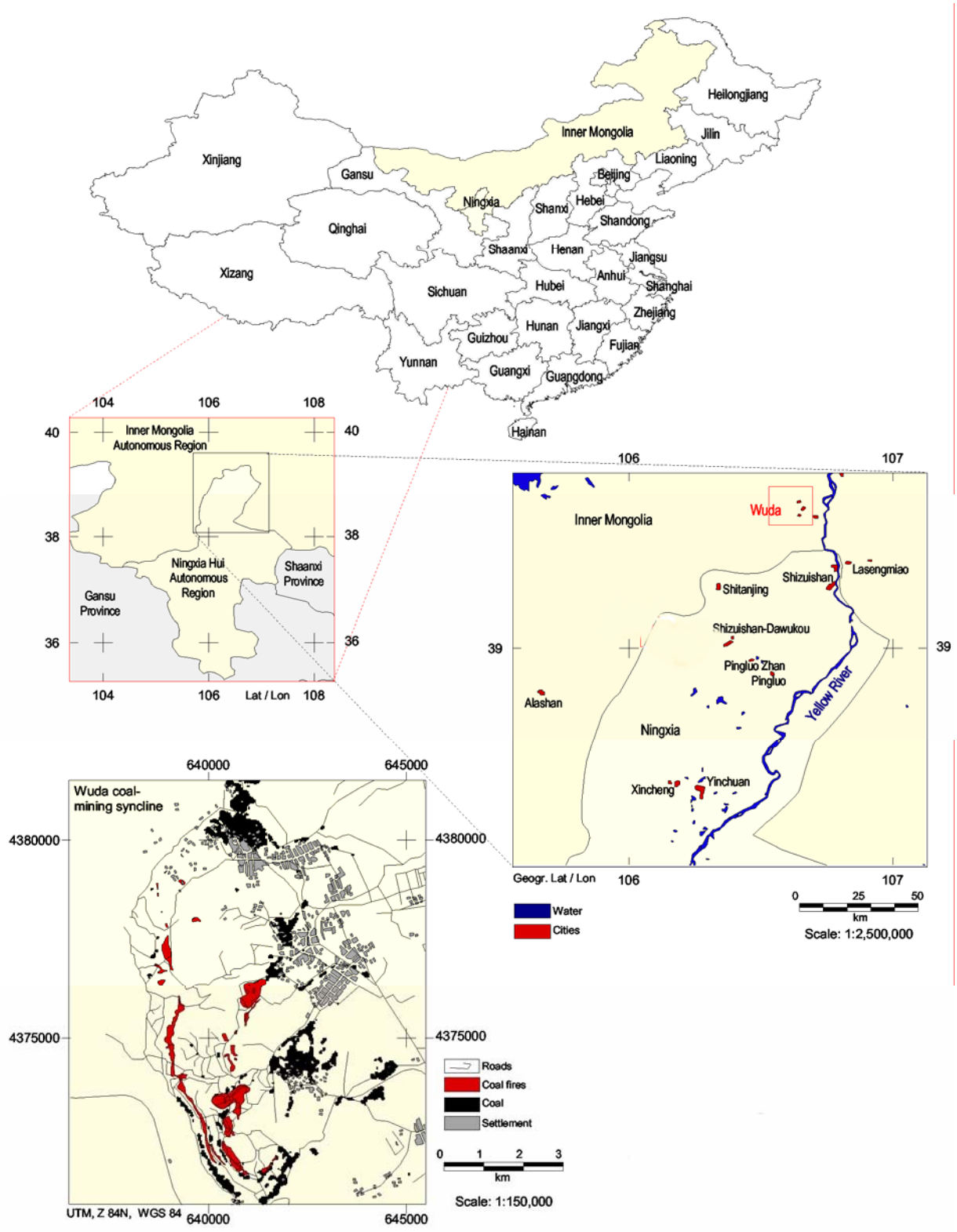

Figure 2.1: Location of the study area in China. The lower left frame shows the Wuda syncline serving as test area for fire probability analysis. Source: KÜNZER (2004)

2.3 Coal fires and coal fire related features

The predominant type of coal fire in the Wuda area is the one of a subsurface coal mine fire. At present 16 such fires are known in the Wuda coalfield covering 3.07 km² or 8.8 % of the total coal mining area. Eight coal seams are burning in depths of up to 100 metres, although most fires are closer to the surface (ZHANG, 2004). Starting from the abandoned cavities (called "goafs") which result from longwall mining, they are spreading along these goafs and into the unexploited seams as long as oxygen supply is sufficient. Oxygen supply is provided by the ventilation system built during exploitation of the respective zone or by cracks due to collapse of the overburden.

Coal fire generated geomorphologic features are a wide spread phenomenon. They include burnt pits, crack systems and pyrometamorphic minerals (figures 2.2 and 2.3). Burnt pits form when a coal fire occurs at the outcrop of a coal seam with a large dip angle, whereas cracks result from subsidence due to fires burning along seams with gentle dip angle. Pyrometamorphic minerals form in the rock adjacent to extraordinary hot fires. If they are exposed on the surface, their yellow - redish colours are often visible in high to medium resolution satellite data (KÜNZER, 2005). Common features observable at cracks are smoke exhalations and a strong rise in temperature in up to one meter distance from the crack. These features are typical for fires burning close to the surface. (ZHANG, 2004; KÜNZER, 2005)

Figure 2.2 : Near surface coal fire and pyrometamorphic rock.

Photos : C. Kuenzer 09/2002

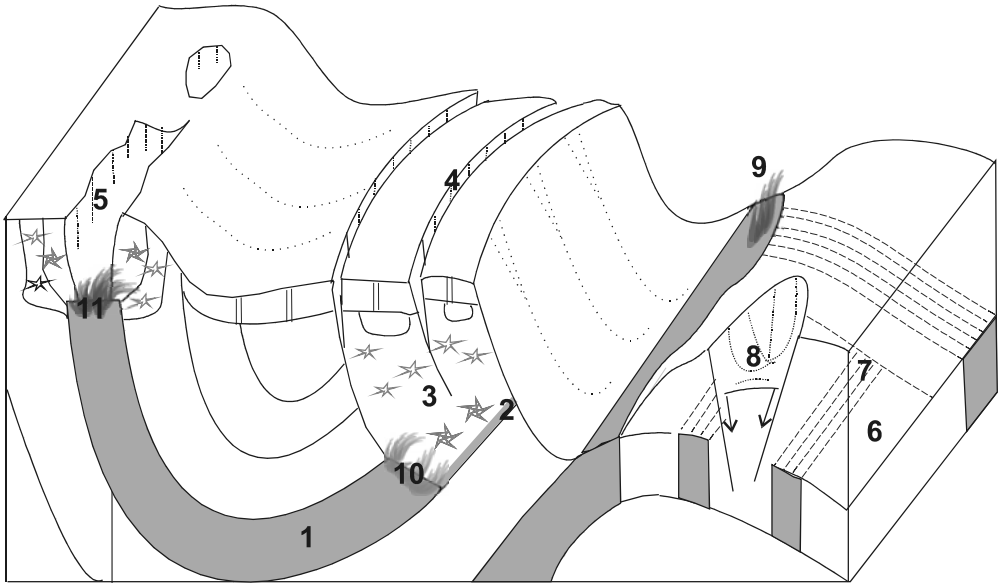

Figure 2.3: Coal fires and their related features. 1 Coal seam; 2 Ash; 3 Pyrometamorphic rock; 4 Crack; 5 Burnt pit; 6 Longwall mining; 7 Pillar; 8 Subsidence 9 Surface coal mine fire; 10: Subsurface coal seam fire; 11: Surface natural fire. Source: ZHANG (2004)

3. Theoretical background

3.1 Dealing with uncertainty in decision making

Decision making is based on a theoretical model of the real world. However, information incorporated in modelling reality tends to be inaccurate, incomplete or ambiguous. Therefore, uncertainty is inevitable in the decision making process. Considering this process as a set membership problem is a useful perspective from which to understand the source and role of uncertainty. The decision frame or frame of discernment contains all decision alternatives (or hypotheses) under consideration and evidence is information through which set membership of an entity in the decision set can be evaluated. Thus, the decision making process contains three basic elements where uncertainty can occur: the evidence, the decision set and the relation that associates the two (EASTMAN, 2003). The latter one of these types, which can be denoted as decision rule uncertainty, belongs to the category of uncertain set membership expression, known as fuzzy measure. The term fuzzy measure includes fuzzy sets, Bayesian probabilities and the beliefs and plausibilities of Dempster-Shafer Theory (DST).

3.1.1 Fuzzy Set Theory and Multi Criteria Evaluation (MCE)

Fuzzy sets are sets without sharp boundaries meaning that the transition between membership and non membership of an entity in the set is gradual. A fuzzy set is characterized by a fuzzy membership grade that ranges from zero to one, indicating a continuous increase from non membership to complete membership. This contrasts with the crisp set exhibiting sharp boundaries. However, a crisp set can also be seen as a special case of a fuzzy set where fuzzy membership changes instantaneously from zero to one.

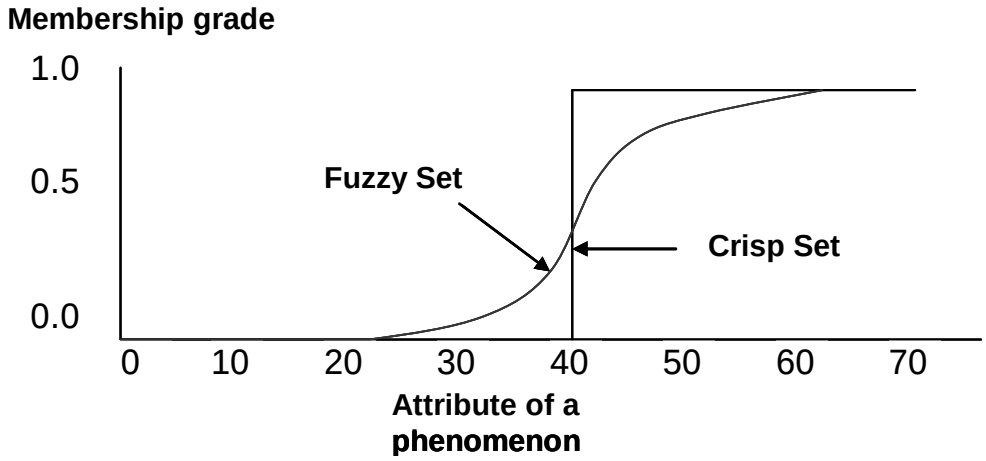

Figure 3.1: Membership functions for crisp and fuzzy sets

Fuzzy sets are commonly used in representing continuous variables in decision problems related to Multi Criteria Evaluation (MCE) (EASTMAN, 2003). MCE is primarily concerned with how to combine the information from several criteria to form a single index of evaluation. In case of boolean criteria or constraints, the solution usually lies in the union or intersection of conditions. However, criteria are often based on continuous phenomena and require fuzzy representation. Fuzzified criteria are then combined using Weighted Linear Combination (WLC) or Ordered Weighted Average (OWA). In WLC criteria are weighted and products of the criterion score with the respective criterion weight are summarized. Establishing factor weights resorts to the pair-wise comparison technique. OWA uses criterion weights similar to the WLC method but in addition a set of order weights assigned to the rank order position of factor values for a given location (SAHOO ET AL, 2001; MALCZEWSKY, 1999)

3.1.2 Bayesian probability theory

When complete information is available or assumed, the primary tool for the evaluation of the relationship between the indirect evidence and the decision set is Bayesian probability theory which is based on Bayes Theorem (EASTMAN, 2003). Bayes Theorem defines a rule on how to combine new evidence about a hypothesis along with prior knowledge to arrive at an estimate of the likelihood that the hypothesis is true. In the notation of probability theory this is

$$p(h|e) = \frac{p(e|h) \cdot p(h)}{\sum_i p(e|h_i) \cdot p(h_i)} \qquad \text{(Eq.1)}$$

Where

p(h|e) = the probability of the hypothesis being true given the evidence (posterior probability)

p(e|h) = the probability of finding that evidence given the hypothesis being true (conditional probability)

p(h) = the probability of the hypothesis being true regardless of the evidence (prior probability)

3.1.3 Dempster-Shafer Theory of Evidence (DST)

The Dempster-Shafer Theory of Evidence (DST) is based on Dempster`s work on the generalization of Bayesian lower and upper probabilities (DEMPSTER, 1967). The lower and upper probabilities represent the belief and plausibility, respectively, that a given body of evidence supports a particular hypothesis (SHAFER, 1976). DST defines hypotheses in a hierarchical structure developed from a basic set of hypotheses {A, B, C} that form the frame of discernment or decision frame $\Theta = \{A, B, C, AB, AC, ABC\}$.

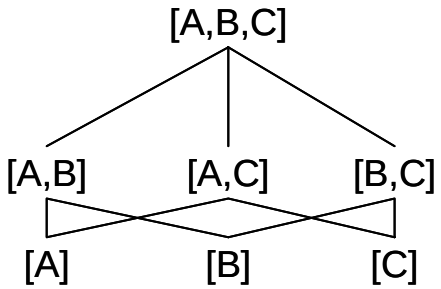

Figure 3.2: Frame of discernment for three singleton hypotheses

[A], [B], [C] are called singleton hypotheses because each of them only contains one element.

The power set of Θ is denoted by

$$2^{\Theta} = \{A \subset \Theta\} \qquad \text{(Eq. 2)}$$

where A is a subset of Θ.

A function $m : 2^{\Theta} \rightarrow [0,1]$ is called a Basic Probability Assignment (BPA) when

$$m(\varnothing) = 0 \quad \text{(Eq. 3)}$$

and

$$\sum_{A \subset \Theta} m(A) = 1 \quad \text{(Eq. 4)}$$

The function m ("mass of belief") is a measure of belief committed to each hypothesis. The total belief committed to a hypothesis H is given by

$$Bel(H) = \sum_{A \subset H} m(A). \quad \text{(Eq. 5)}$$

The function Bel: $2^{\Theta} \to [0,1]$ is called a Belief Function (Bel) over Θ if it satisfies the conditions:

$$Bel(\varnothing) = 0 \quad \text{(Eq. 6)}$$

$$Bel(\Theta) = 1 \quad \text{(Eq. 7)}$$

And for every positive integer n and every collection of hypotheses A_1, A_2 ,…, A_n of a subset of Θ

$$Bel(A_1 \cup \ldots \cup A_n) \geq \sum_{\substack{I \subset \{1 \ldots n\} \\ I \neq \varnothing}} * (-1)^{|I|+1} Bel(\cap_{i \in I} A_i) \quad \text{(Eq. 8)}$$

The Plausibility function Pl: $2^{\Theta} \to [0,1]$ is defined using the Belief Function Bel as:

$$Pl(H) = 1 - Bel(\overline{H}),$$

$$= \sum_{A \subset \Theta} m(A) - \sum_{A \subset \overline{H}} m(A),$$

$$= \sum_{A \cap H \neq \varnothing} m(A) \quad \forall H \subset \Theta \text{ where } \overline{H} \text{ is the negation of H} \quad \text{(Eq. 9)}$$

Belief and plausibility represent the lower and upper boundary of the commitment to H. Metaphorically speaking belief denotes all the accumulated "hard" evidence in support of H, whereas plausibility represents the grade to which H cannot be rejected.

The degree of uncertainty about H is thus represented by the difference

$$Pl(H) - Bel(H). \quad \text{(Eq. 10)}$$

The difference is called belief interval. When the degree of uncertainty equals 0, then

$$Bel(H) + Bel(\overline{H}) = 1, \quad \text{(Eq. 11)}$$

which is the Bayesian probability. The relationship between belief, plausibility and belief interval is illustrated in figure 3.3

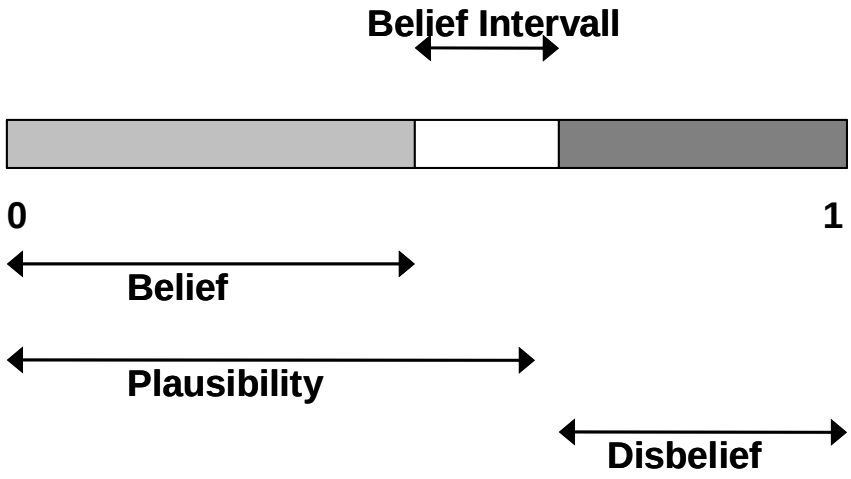

Figure 3.3: Relationship between belief, plausibility and belief interval

Belief Functions representing distinct bodies of evidence can be combined by means of Dempster's rule of combination which implies the orthogonal sum of the belief functions:

$$m(H) = (1-k)^{-1} \sum_{A,B \subset \Theta : A \cap B = H} m_1(A) m_2(B) \qquad \text{(Eq. 12)}$$

where

$$k = \sum_{A,B \subset \Theta : A \cap B = \varnothing} m_1(A) m_2(B) \qquad \text{(Eq. 13)}$$

K is the amount of total probability committed to disjoint (contradictory) subsets of Θ and therefore represents a measure of conflict between two bodies of evidence. When k equals to 1, the bodies of evidence are completely contradictory and their orthogonal sum does not exist.

A geometric interpretation of the orthogonal sum is shown in figure 3.4. A_i and B_j are subsets of Θ associated with BPAs. They are called focal elements of the belief functions $s_1 = \{A_1,\ldots,A_i\}$ and $s_2 = \{B_1,\ldots,B_j\}$. The width of the columns and rows is proportional to the BPA associated with the focal element. Each intersection is assigned the product of the corresponding masses and the contributions of coincident intersections are summed.

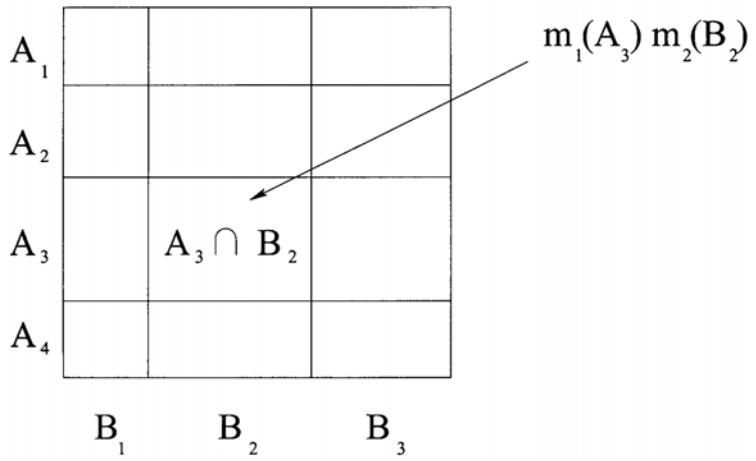

Figure 3.4: Dempster's rule of combination . From Cuzzolin (2004).

3.1.4 Key differences

In contrast to Fuzzy Set Theory, Bayes and Dempster-Shafer logics are both concerned with the substantiation of crisp sets. Fuzziness in the latter two relate to the relationship between the evidence and the decision set, the strength of which is in doubt. The primary difference between Bayes and DST concepts is characterized by the way of dealing with the absence of evidence: Bayes considers the absence of evidence in support of a hypothesis to constitute evidence in the support of the counter hypothesis, whereas DST does not. Thus, despite the fact that both consider the decision frame to be exhaustive, DST considers the possibility of ignorance whereas Bayes does not (EASTMAN, 2003). DST also includes multi element hypotheses in recognition of the fact that evidence often supports the combination of hypotheses without the ability to further distinguish between their subsets.

3.2 State of knowledge

3.2.1 Recent advances in DST

ZADEH (1984) demonstrated the limitations of the Dempster's rule of combination in the case of highly conflicting evidence. He presented an intriguing example of a patient who is examined by two physicians. Physician A diagnoses meningitis (M) with 99% probability whereas physician B diagnoses concussion (C) with 99% probability. Both agree on a low probability of 1% for a brain tumor (T). According to equation 12

the degree of conflict k is 0.9999, and the normalization factor 1 - k is 0.0001. Using DS rule of combination, the following results are obtained:

Table 3.1: Beliefs in Zadeh's physician patient example

	m_A	m_B	Dempster's Rule	Max operator (YAGER, 2004)
Meningitis (M)	0.99	0.00	0.00	0.497
Brain tumor (T)	0.01	0.01	1.00	0.005
Concussion (C)	0.00	0.99	0.00	0.497
Θ	0.00	0.00	0.00	0.000
Ø	0.00	0.00	0.00	0.000

These results are counterintuitive, as 99.99% evidence is neglected due to conflict. To overcome this problem, various approaches have been presented. The rule proposed by DUBOIS & PRADE (1988) proposed to transfer conflicting belief masses to the union of the respective supported hypotheses whenever the intersection of these hypotheses produces an empty set. DEZERT & SMARANDACHE (2003) employed what they called a hyper power set. The hyper power set also includes the union and intersection of hypotheses to allow for paradoxical information. Given a frame of discernment Θ = {A, B} with only two singleton hypotheses, then probability assignment has to satisfy the condition

$$m(A)+m(B)+m(A\cup B)+m(A\cap B)=1 \qquad \text{(Eq. 14)}$$

Hence, in contrast to original DST, the elements of the frame of discernment have not necessarily to be mutually exclusive. JØSANG (2002) introduced a consensus operator replacing traditional Dempster rule of combination. Given contradictory opinions of two independent observers after two different observation periods, this operator in a figurative way represents the opinion an imaginative agent would have after having observed the process during both periods. YAGER (2004) proposed the use of disjunctive operators, which are less strict. Equations 11 and 12 are modified accordingly as

$$m(H)=(1-k)^{-1}\sum_{A,B\subset\Theta:A\cap B=H}\max\left[m_1(A)m_2(B)\right] \qquad \text{(Eq. 15)}$$

$$k = \sum_{A,B \subset \Theta : A \cap B = \varnothing} \max\left[m_1(A) m_2(B)\right] \qquad \text{(Eq. 16)}$$

In the physician – patient example, the new diagnosis would then be

$m_{A,B}(M) = 0.497$, $m_{A,B}(C) = 0.497$, $m_{A,B}(T) = 0.005$ (see table 3.1).

Up to now no consensus has emerged as to which of the proposed methods are to use in case of highly conflicting evidence (CORGNE ET AL, 2003). It is common practice to estimate the degree of conflict beforehand and to set a threshold level beyond which the decision delivered by Dempster's rule is refuted. This of course raises the question of how to define this threshold. Usually, past experience or expert knowledge are involved in determining the threshold (CORGNE ET AL, 2003). However, when ignorance is assumed, the original combination rule gives reliable results. Table 3.2 shows the results for the above example given a minimum amount of ignorance.

Table 3.2: Beliefs in the physician patient example when ignorance is assumed

	Physician A	Physician B	Dempster's Rule
Meningitis (M)	0.98	0.00	0.490
Brain tumor (T)	0.01	0.01	0.015
Concussion (C)	0.00	0.98	0.490
Θ	0.01	0.01	0.005
Ø	0.00	0.00	0.000

3.2.2 Brief overview: application of probability theory in spatial problems

Methods of handling uncertainty are increasingly gaining access to spatially related decision support. This is especially true for the Fuzzy Set Theory that is broadly applied in multi criteria analysis techniques such as MCE (EASTMAN, 2003). But as to now less attention has been paid to decision rule uncertainty. Whereas Bayes and Dempster-Shafer theories are already routinely being applied to decision problems in

various fields, in particular micro electronics to medicine, they are not yet fully established in spatial geographical decision problems. Some approaches to combine probabilistic models with GIS origin in the field of geologic hazard mapping and resource exploration. The weights of evidence method initially developed by BONHAM-CARTER ET AL. (1988, 1989) for evaluation of gold bearing potential is a spatial interpretation of Bayes Theorem. Within this framework probabilities are based on spatial relation between the features used as indicators or predictors and known gold deposits. The approach is therefore also denoted as data-driven, in contrast to knowledge-driven approaches, which derive probabilities exclusively from expert knowledge on the relationship between the indicators and the event or hypothesis to be predicted (CARRANZA & HALE, 2002). LEE & CHOI (2004) used this model to evaluate landslide susceptibility based on multiple geologic, geomorphologic and landcover factors ("predictors") in a GIS. Weights for the predictors were derived from Bayesian posterior probabilities for a landslide event to occur within or outside the predictor pattern. The posterior probability was quantified by the degree of spatial intersection between documented landslide occurrences and the area where the predictor is present. Weights were finally summed to form the susceptibility maps. Other applications of this theory to mineral potential mapping can be found in CHUNG & FABBRI (1993). CARRANZA & HALE (2002) combined evidential belief functions of spatial geological evidences to evaluate gold bearing potential. Belief functions are modified Dempster-Shafer belief functions which take into account the spatial relationship of an evidential data layer and known gold deposits on one side and the relationship among the subsets of spatial evidences within an evidential data layer on the other side. Practically, zonated distance maps for the evidence features were intersected with known gold deposits to derive weights for different proximity zones. A similar approach was used to map porphyry copper potential (TANGESTANI & MOORE, 2002). HUBERT-MOY ET AL. (2002) estimated the winter season land cover pattern in an intensively cultivated region based on multiple geo- and cultivation related indicators, which they fused according to Dempster-Shafer Theory of Evidence. Probability weights for the indicators were derived combining expert knowledge and time series of past landcover data obtained from remote sensing.

Rising awareness for uncertainty in decision making is also reflected in recent developments on the GIS software market. IDRISI Kilimanjaro™ software by Clarks Labs, a GIS mainly designed for analysing raster data features a sophisticated decision

support toolset including the modules Fuzzy to generate probabilities and belief to carry out Dempster-Shafer Analysis on specified input data (EASTMAN, 2003).

3.3 Summary

Three methods to deal with decision rule uncertainty were introduced: Fuzzy Set Theory, Bayes Theorem and DST. Whereas fuzzy sets denote the uncertainty in the definition of a criterion, Bayesian and Dempster-Shafer Theories apply to cases where the evidence does not directly and perfectly imply the decision set under consideration. Both logics define a set of decision alternatives denoted as hypotheses and combine different pieces of evidence to determine membership of an entity in the hypothesis. However, they differ in the way of dealing with absence of evidence.

Recent research has revealed the weakness of Dempster-Shafer rule of combination in dealing with highly conflictive evidence. Different approaches to overcome this problem were briefly discussed.

Finally, a brief overview on applications of both theories was given with focus on spatial decision problems, in particular geohazard mapping and geological resource mapping.

4. Data sets

4.1 Surface Temperature Measurements

In three field campaigns in 2003, 2004 and 2005 temperature measurements were conducted by DFD scientists in the vicinity of known and assumed fire locations. A hand held infrared radiometer was used, which allows for measurement of temperatures by measuring the radiant temperature of a body. The radiant temperature is a measure for the electromagnetic radiation resulting from collisions between the particles in random motion denoted as Brownian motion. It is linked to the kinetic temperature via the emissivity of the emitting body. The kinetic or internal temperature in turn expresses the strength of the Brownian motion.

Sample design was not based on regular or statistical pattern, instead measurements were made at fractures or cracks encountered during the field inspection. Measurements were repeated in a few day's interval to account for different soil moisture and wind conditions and maximum and average temperatures were noted. The exact coordinates of the measurement points were determined with a pocket GPS and transferred into an ESRI point shape file together with the temperature values.

4.2 Thermal anomalies

All matter radiates energy at thermal infrared wavelengths (3 to 15µm). For an object at a constant kinetic temperature, the radiant energy varies as a function of wavelength. With increasing temperature, the total amount of radiant energy increases and the radiant energy peak shifts towards shorter wavelength. This shift is described by Wien's displacement law. Thermal anomalies induced by subsurface fires in the study area range between 30 °C (303 K) which is only few degrees above the daytime background, and more than 300 °C (~ 573 K) (ZHANG 2004; HIRNER, 2005 PERS. COMM.).

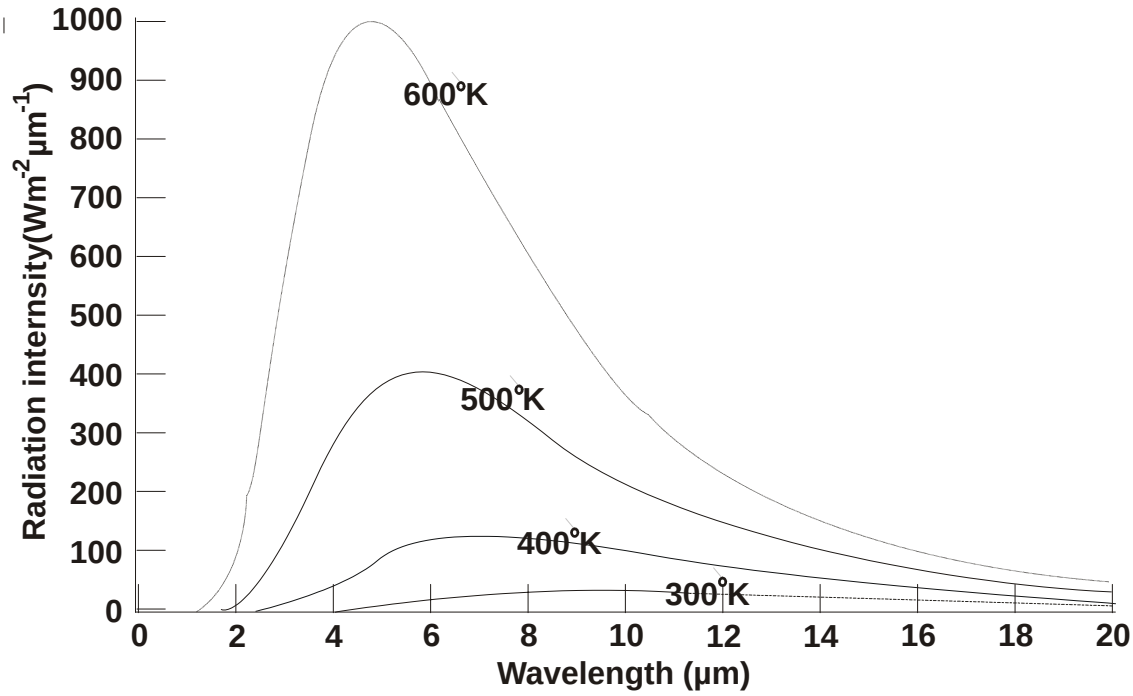

Figure 4.1: Spectral distribution curves of energy radiated from black body radiators at different temperatures. From ZHANG (2004)

Figure 4.1 shows that at temperatures below 100°C (~ 373 K), emission in the near (NIR 0.75 – 1.5 µm) and middle (MIR 1.5 - 3 µm) infrared is not significant. Moreover, the reflective part of the solar radiation increasingly masks the emitted radiation in the NIR domain. Hence, the thermal infrared (3 - 100 µm) has proved to be most suitable to detect both, low as well as high amplitude thermal anomalies in thermal remote sensing data (ZHANG, 2004). The Enhanced Thematic Mapping (ETM+) sensor on board LandSat 7 (LS7) records thermal infrared radiation in the spectral band 10.4 to 12.5 µm (band 6) with a spatial resolution of 60 m. The band is located in a part of the TIR range where the incoming solar radiation is not absorbed by the atmosphere (atmospheric window)

The raw (DN-value) LS7 band 6 image serves as input for an algorithm to automatically extract coal fire induced thermal anomalies (ZHANG, 2004). Using a moving window technique, pixels are classified as anomalous according to their position in the subset histogram. The threshold for separation of anomalous pixels is derived from a detailed analysis of the thermal signature of known coal fires in LS7 ETM+ data and then determined dynamically for the respective subset histogram. Anomalous pixels are clustered based on neighbourhood analysis. Anomaly clusters caused by different sources, such as uneven solar heating, water bodies or industry are removed by investigation of statistical parameters of the clusters in comparison to their

background. The result is a bit map with the value 1 for anomalous pixels and zero for the background. In the underlying thesis a bit map derived from a LS7 ETM+ night scene of the Wuda Region acquired in 2003 was used. Night time data is especially suitable because of the absence of solar heating effects. The bit map was converted into an ESRI polygon shape file using the Arc Toolbox Raster to Feature Conversion Tool.

4.3 Cracks

Cracks were digitized in ArcMap from a Quickbird scene of the study area acquired in 2003. The panchromatic channel has a spatial resolution of 0.6 m which is sufficient to detect linear objects with a width of a few decimetres, given they have a length of several metres. The width of fire and mining induced cracks in the Wuda syncline varies between 0.1 and 2.5 m; their length can reach up to 1000 metres.

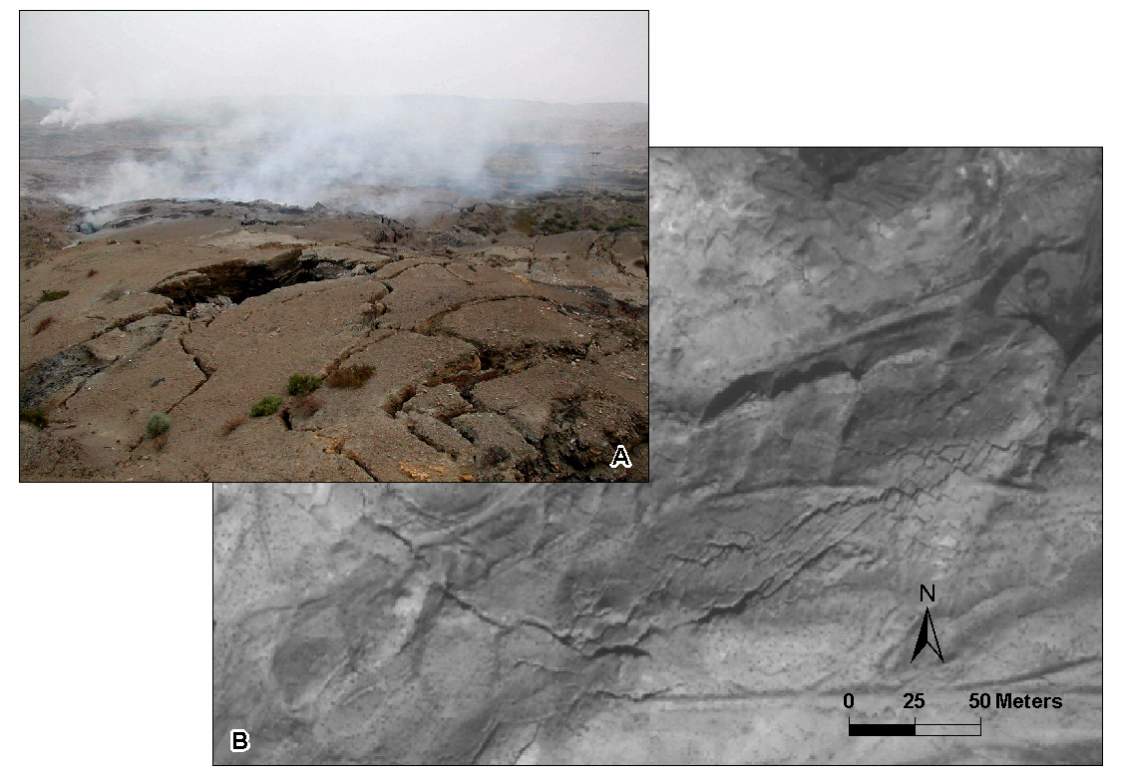

Figure 4.2: Fire induced cracks in the Wuda coal field (A) and on the Quickbird panchromatic Scene acquired in 2003 (B) Photo: C. Kuenzer

4.4 Longwall mining

Long wall mining is a common mining technique used in the Wuda mining area. A cutting head moves back and forth across a panel of coal some hundred m in width and up to two thousand metres in length (figure 4.3). The cut coal falls onto a flexible conveyor for removal. (UMWA, 2005) The roof in the remaining goafs ("gobs") isn't supported any longer, which often leads to collapse of the overburden. At surface large area subsidence of up to 14 m in vertical direction can be observed (LITSCHKE, 2005 PERS. COMM.)

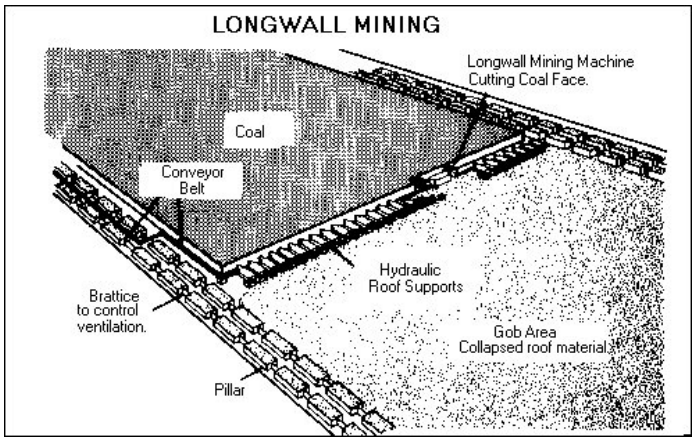

Figure 4.3: Longwall mining technique. Source: UMWA (2005)

The shapes of the goafs were digitized from an analogue mining map and provided as ESRI polygon shape file by LITSCHKE (2005). The map was provided by the Shenhua Group Corporation, the mining company operating the Wuda mines.

4.5 Mining activity

Mining activity was derived from the year 2003 Quickbird panchromatic scene through visual interpretation. Recognizable features related to mining activity include coal storage and coal waste piles, mining entrances and cliffs produced by open cast mining (figure 4.4). Each of the identified features was marked by a point on the satellite image and the points with their geometric properties were stored in ESRI point shape file format.

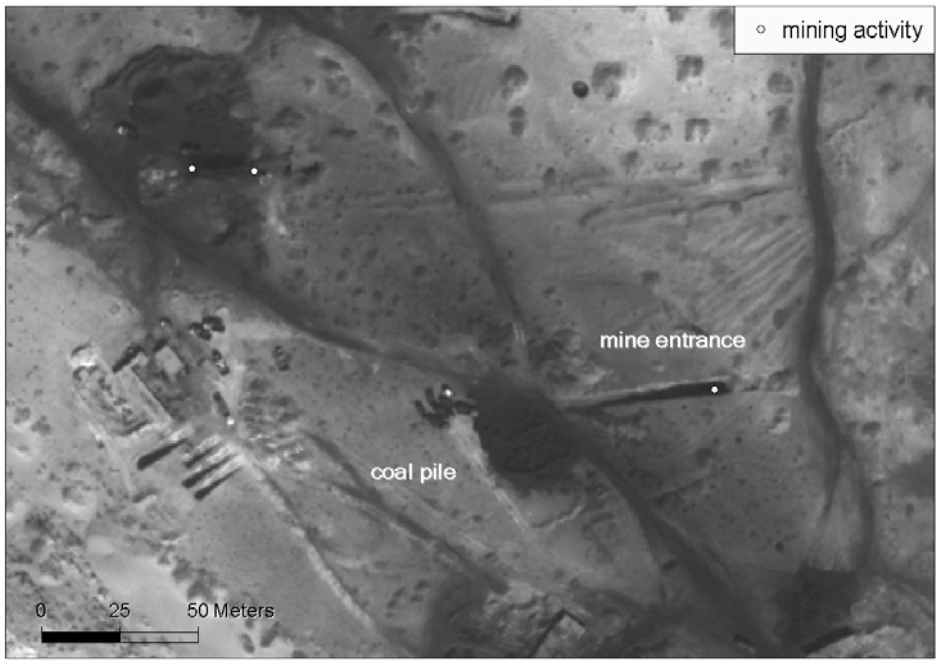

Figure 4.4: Mining related surface features visible in the Quickbird panchromatic Scene of 2003

4.6 Coal seam outcrops

A geological map of the Wuda syncline was available from the Shenhua Group which clearly showed the delineation of coal seam outcrops. These outcrops were digitized in ArcMap and stored in a ESRI line shape file. The sedimentology was studied in field trips by DMT scientists in 2003 (GIELISCH, 2004).

4.7 Known fires

Information about location and extent of subsurface coal fires in the Wuda coal mining area is based on knowledge of local mining engineers and mine administrators who have already been monitoring fires over the past decade. In 2000 an assessment of the fire boundaries by aerial photography and GPS measurements was undertaken on the Chinese side (KÜNZER, 2005). Thermal field measurements and borehole drillings completed these activities. In the years 2003 to 2005 scientists from DFD conducted extensive temperature measurement campaign at known fire locations to actualize the fire extents and to study fire dynamics (KÜNZER & HIRNER 2005 PERS. COMM.). The aggregated information was available as fire extent polygons in ESRI shape file format.

Within this thesis the known fires serves as “ground truth” data to validate the results of fire probability evaluation.

4.8 Summary

Six data sets indicative for coal fires were incorporated in this thesis:

- measured surface temperatures collected during field campaigns in the study area,
- thermal anomalies automatically extracted from LS7 TIR data,
- surface cracks digitized from Quickbird satellite imagery,
- distribution of subsurface mining activity digitized from maps,
- surface features of mining activity digitized from Quickbird satellite imagery
- and occurrence of coal seam outcrops digitized from maps.

A map with the year 2004 status of existing fires, compiled from combined field investigation and aerial photography was used for validation of the results.

5. Conceptual framework and methodology

Modelling occurrence and distribution of coal fires can be viewed as a decision problem. In particular, the decision pertains to the question if a given spatial geographical entity (e.g. a raster cell) is a member of the elements (here the assumptions that a fire is present or absent) in the decision set. The indicators described in chapter 4 then constitute the evidence upon which the membership of an entity in the decision set is determined. The decision set it self is crisp if there are only two meaningful decision alternatives concerning the presence of a fire: “yes” or “no”. These alternatives correspond to the hypotheses within probability theory. Uncertainty here emerges in the relation between the evidence and the decision set, as will be discussed in detail in section 5.3.2. Generally speaking, the available evidence is often weak or even ambiguous and the absence of evidence in favour of one hypothesis can’t be used as evidence for the counter hypothesis. Considering this, DST constitutes a suitable approach to model coal fire probabilities. Uncertainty is then translated into a probability for the hypothesis to be true given the evidence. Furthermore, probabilities and their aggregated form belief constitute the demanded parameter to abstract fire relevant information from the different data sets.

Other models to be considered in the framework of modelling fire probabilities are MCE or Bayesian probability theory. In MCE, decision rule uncertainty might be expressed through criterion weights, too. Weak indicators corresponding to high uncertainty would then be assigned low criterion weights and vice versa. Yet, the superiority of DST compared to MCE is based on the fact that not every available indicator has to be used as evidence for the presence of a fire. Instead, ambiguous or weak indicators such as distribution of coal deposits can also be used as evidence for the counter hypothesis, absence of a fire, in turn further refining evidence for the hypothesis „fire“. If coal seam distribution was to be incorporated in an overlay technique it could only be assigned a weak probability for the hypothesis „fire“, thus providing only little additional information.

Although Bayesian probability theory accounts for uncertainty in the decision set membership it doesn’t allow for ignorance. Ignorance is associated with the majority of the present indicators, however. The presence of a crack for example points to a fire with a probability p higher than zero and lower than one. According to Bayes the

remainder of the probability 1- *p* has to be taken as evidence for the absence of a fire. This is in contradiction to reality, for it is known that

- not every fire produces cracks,
- cracks are caused by other processes than fires and
- cracks might simply have been ignored in the satellite data.

In other words cracks simply don't let for statements as to the absence of a fire. Consequently the remainder of the probability 1- *p* resulting from presence of a crack can not be assigned to one of the singleton hypotheses. It rather represents the portion of ignorance in the decision process.

5.1 Modelling uncertainty in spatial data

Applying DST to spatial decision problems means introducing an additional spatial component of uncertainty into the relation between the evidence and the hypothesis. Not only might a given indicator point to a hypothesis with a probability less than one, this probability will also vary with the distance from the indicator features. This is particularly true in the context of coal fires, where the characteristics of the indicators can only be retrieved from the surface whereas the inducing fire is located within unknown distance below the surface. The indicator features (from which evidence is derived) are linked to their cause (upon which statements are to be made) via distant effects through the spatial dimension, which is not accessible to measurement. It is the particular geometric expression of these distant effects that constitutes the actual source for spatial uncertainty. Probability distribution at surface can then be seen as a consequence of projecting the three dimensional spatial relation between evidence features and source into the surface plane.

Within the scope of this study probability has been defined in terms of the probability for a fire being located perpendicular underneath a considered location (e.g. a raster cell). In terms of probability theory, the value assigned to each raster cell denotes the probability or grade to which this cell is a member of the considered decision set element or hypothesis. The membership is a function of distance which is illustrated in figure 5.1.

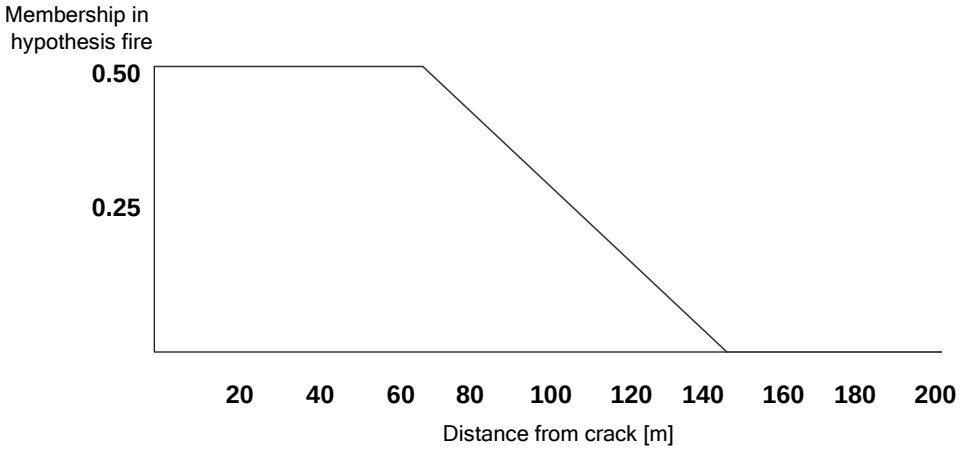

Figure 5.1: Membership function for the crack data set

This definition principally does not imply any information about the fire depth. However, as will be explained in section 5.3.2 the temperature measurements allow for assumptions about the fire depth to a certain degree. Hence, where this indicator mainly contributes to a high belief in the presence of a fire, proximity to the surface can be assumed.

Fires are a three dimensional phenomenon and so is the probability for these fires. However, because indicators included in this study were available only as two dimensional feature data, fire probability was modelled in two dimensions.

5.2 Setting up the frame of discernment

The decision space in the at hand decision problem contains two basic or singleton hypotheses: “fire” or “no fire”. Within the frame of DST the union of these singleton hypotheses, which represents incomplete knowledge within the decision, has to be considered, too. The frame of discernment is presented in figure 5.2.

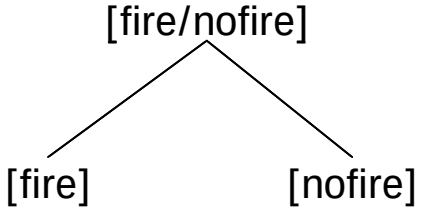

Figure 5.2: Frame of discernment for the decision problem in the context of coal fire probability modelling

5.3 Generation of probability maps

Dealing with uncertainty in spatial modelling requires spatial representation of this uncertainty. In terms of DST, probabilities assigned to the evidence and beliefs and plausibilities are then represented as spatial distributions. Management and visualization of spatial information through maps is one of the expressed strengths of GIS. On this background maps were expected to be a suitable medium to visualize the single and combined evidence from fire indicators.

5.3.1 Determination of basic probability weights

A key issue is to derive probability weights for a given evidence dataset to reflect decision rule uncertainty. As discussed in section 3.2.2, two possibilities come into question: a data-driven or a knowledge-driven approach. The former approach derives possibilities based on the relation between the evidence features and the known fire locations which, in its simplest form can be expressed as

$$m(S_i) = \frac{A(T) \cap A(S_i) \neq \varnothing}{A(S_i)}, \qquad \text{(Eq. 17)}$$

where

$m(S_i)$ is the probability mass given by the evidence S_i

$A(S_i)$ is the total area of the evidence S_i pointing to the hypothesis under consideration;

$A(T)$ is the area where the hypothesis is known to be true.

However, this approach requires at least two dimensional data. This is true only for the longwall mining and the thermal anomaly data, which are polygon feature type. The remainder of the data comprises point or line feature type. For these data types, topological measures based on the ratio of evidence features lying within or touching the known fire zones and the total feature number could be employed. Both approaches require a priori knowledge on existing fire zones. Although this knowledge is available for the study area, it can't be presumed for potential transfer regions. To make the the algorithm transferable to less intensely investigated coal mining areas probability weights should therefore not depend on knowledge of existing fires.

In contrast, a knowledge-driven approach takes into account the causal relations between evidence data and the supported hypothesis. Taking the crack evidence data as an example, it is known that both, subsurface fires and subsurface mining have to be equally considered. Thus, when prior information on existing coal fires and distribution of underground mining is missing, an equal probability for both causes is intuitive.

Probability weights within this study were derived using a simple knowledge-driven approach. Basically, indicators were classified and weighted according to the degree to which an indicator points to a hypothesis. The degree or strength takes into account the number of possible causes for the evidence features to occur. In identifying possible causes expert knowledge came into play. Technically, the maximum probability was divided by the number of these causes. Hence, a first class indicator characterized by a basic probability of one must satisfy the condition of mono causality with respect to coal fires. This implies a zero decision rule uncertainty. A second class indicator can have two or more causes one of them being a coal fire. Decision rule uncertainty ranges between zero and one and the probability mass is reduced according to the number of plausible causes. Finally, a third class indicator rather constitutes a risk factor than a direct indicator and is assigned an fixed value of 0.25 for the probability mass. Table 5.1 shows the classification of the available data sets.

Table 5.1: Classification scheme for coal fire relevant indicators used in this thesis

fire			**nofire**	
Class	Evidence set	BPA	Evidence set	BPA
1- unambiguous indicator	surface temperature data	1	Coal deposits	1
2 - ambiguous indicator	thermal anomalies, cracks	0.5		
3 - weak indicator or indirect indicator	longwall mining, mining activity	0.25		

The chosen approach helps to ensure transferability through equally weighting any of the possible causes as long as absence of priori knowledge about the abundance of the causes is assumed.

5.3.2 Assigning spatial probability functions to the datasets

The following chapter deals with the spatial component of uncertainty. This component results in probability distributions the geometry of which was derived from expert knowledge. First, the physical relation between coal fires and the respective evidence features will be described for a given data set. Conclusions for the geometric characteristics of the probability distribution will then drawn in a second step. Finally the procedure to generate the input probability map for the Dempster-Shafer analysis from an evidence feature dataset will be highlighted. This procedure generally involved distance raster creation from the feature dataset and subsequent standardization of the distances to values ranging from the respective maximum probability to zero. In doing so, a specific fuzzy membership function was used expressing the respective geometric relation between indicator features and combustion zone. The prototype flow scheme is given in figure 5.3.

The core geoprocessing functions mentioned in the following sections will be described in section 6.1.2.

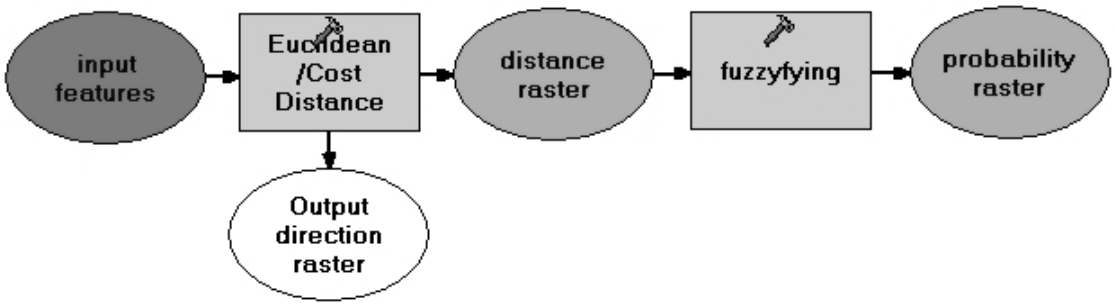

Figure 5.3: Flow scheme for probability map generation in ArcGIS ModelBuilder

Cracks

As a result of the combustion process mass is lost in the form of gaseous combustion products mainly carbon oxides. The emerging voids cause mechanical stress in the adjacent rock leading to collapse and subsidence of the overburden. Depending on the magnitude of the subsidence and the rock type, cracks can develop. As previously explained coal mining is another cause for subsidence related cracks. It is very difficult to distinguish between these two types of cracks on the Quickbird image without prior knowledge of the location of sub surface fires or mining activity. Cracks

were therefore considered as ambiguous indicator for the hypothesis „fire“ with a basic probability mass of 0.5.

The schematic illustration in figure 5.4 shows the geometric relation between the subsurface fire front and its induced surface cracks. The maximum angle α enclosed by the plumb line between the fire front and top ground surface and the line connecting the fire front and the most distant crack in propagation direction of the fire front is 45° (ZYBELL, TU BERGAKADEMIE FREIBERG 2005 PERS. COMM.). Assuming a common fire depth of up to 75 m (GIELISCH, 2004) implies that the fire front can be located anywhere within 75 m distance around a given crack. Translated into probabilities, every crack is surrounded by a circular zone of 75 m where the probability for a subsurface fire to occur within a depth of 75 m is 0.5. As the occurrence of fires is assumed to decrease below depths of 75 m, so does the probability for a fire to be situated outside the 75 m zone. The probability map therefore comprises a 75 m buffer zone with a constant probability value of 0.5 and a linear transition zone of another 75 m where the probability value diminishes to zero.

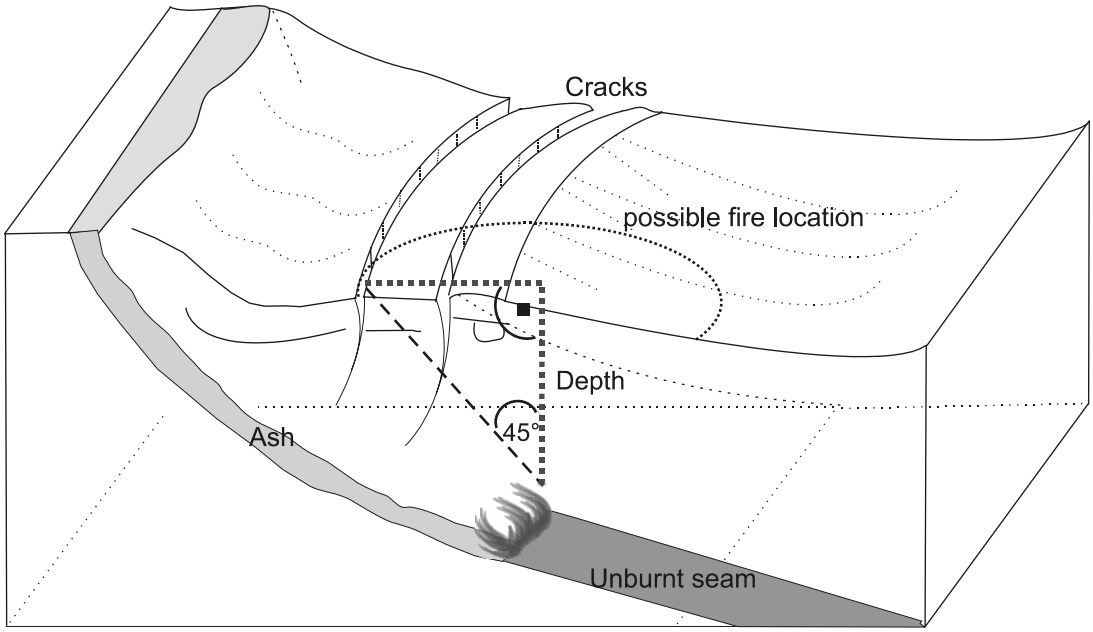

Figure 5.4: Geometric relation between the subsurface fire front and surface cracks

The distance raster for the crack dataset was created with the Euclidean Distance Tool of Spatial Analyst in ArcGIS. It was then converted into a probability raster using the Spatial Analyst Single Output Map Algebra Tool. The conditions were :

- for distance < 75 assign constant value of 0.5;
- for 75 < = distance < 150 assign result of (distance - 150 / (- 150);

- for distance > = 150 assign constant value of 0.

In the above as well as in the following map algebra syntaxes, distance denotes the cell value in the Euclidean distance raster generated from the respective input shape file. The corresponding map algebra syntax can be found in table A1 in the appendix.

Temperature measurements at the surface

Two mechanisms are responsible for the transport of energy produced by a subsurface fire to the surface: convective transport by the exhaust gases and conduction through the cape rock. Convection produces a strong thermal signal with very small spatial extent and is bound to cracks and funnels. Conduction is much slower and tends to produce a less distinct thermal signal with rather large area. For a given surface element temperatures significantly higher than those of the background are a clear evidence for the presence of a subsurface fire. Although the presence of a fire is not in doubt, the exact position of the combustion zone is more difficult to determine. Conclusions as to the position of the fire front can only be drawn from the magnitude of the temperature anomaly. Despite of low amplitude variations due to wind speed, wind direction and recent precipitation patterns (LITSCHKE, 2005; HIRNER, 2005 PERS. COMM.), fire depth is the factor with the strongest influence on the measured temperature anomaly. Thus, high temperatures are a strong evidence for a near surface fire with strong oxygen supply, whereas poorly expressed temperature anomalies point to a greater fire depth. Principally, the temperature data were assigned a basic probability mass for the hypothesis „fire“ of 1 which might strongly be modified according to the value of the recorded temperature, however.

Determination of the probability distribution was based on the assumption that temperatures were mainly measured at cracks. Therefore, the geometric relationship between cracks and the combustion zone has to be true in general also for the temperature data. However, the magnitude of the anomaly yields some information on the fire depth to be considered. Since the fire depth controls the range where cracks can principally occur (figure 5.4) the probability emanating from a temperature measurement has to be modified according to the magnitude of the measured temperature. For example, cracks produced by fires close to the surface are restricted to a smaller radius around the combustion zone. Hence, for measurement points with high

temperatures the probability for the fire front to be located within close horizontal distance to this point approximates one. The probability mass is in a figurative way concentrated in a small area with high values around the point. The reverse conclusions can be drawn for low temperature observations: the fire front can now be assumed in greater depths and the probability that it is located exactly below the crack where the measurement took place decreases.

Technically, the probability function comprised two components. A 75 m buffer zone with constant probability value of 0.75 and an adjacent transition zone of 75 m with decreasing probabilities takes into account the geometric relationship between the combustion zone and the cracks. The constant value of 0.75 reflects the fact that coincidence of a crack and a measured temperature anomaly is a stronger evidence for the presence of a fire than a crack alone. Moreover, an element was included that modifies the zone with constant value of 0.75 according to the measured temperature. That is depending on the temperature the probability emanating from a measurement point is enhanced or reduced within the initial zone boundaries, resulting in a final range between ~ 0.4 and 1

The workflow for generating the probability map from temperature field data deviated from the general scheme. In detail, the following steps were included:

- Creation of an Euclidean distance raster from the temperature data shape file.
- Conversion of the Euclidean distance raster into a probability applying the following conditions map algebra
    - for distance < 75 assign constant value of 0.75;
    - for 75 < = distance < 150 assign result of (distance - 150 / (- 100);
    - for distance > = 150 assign constant value of 0.

Note, that the same diameters as for the crack data were used, since most of the measurements took place at cracks!

- Creation of a kernel density raster from the maximum temperature measured at each data point. The search radius was set to 200 m to ensure a smoothend distribution. Normalization of the density raster cell values to a range of 0 to1.
- Summation of the density raster and the probability raster and normalization of the result to a range of 0 to 1 according to equation 20 to obtain the final probability raster.

$$temperature\_probability = \frac{\frac{density\_raster}{MAX(density\_raster)} + fuzzydist\_raster}{MAX(\frac{density\_raster}{MAX(density\_raster)} + fuzzydist\_raster)}$$

(Eq. 18)

The process is summarized in figure 5.5

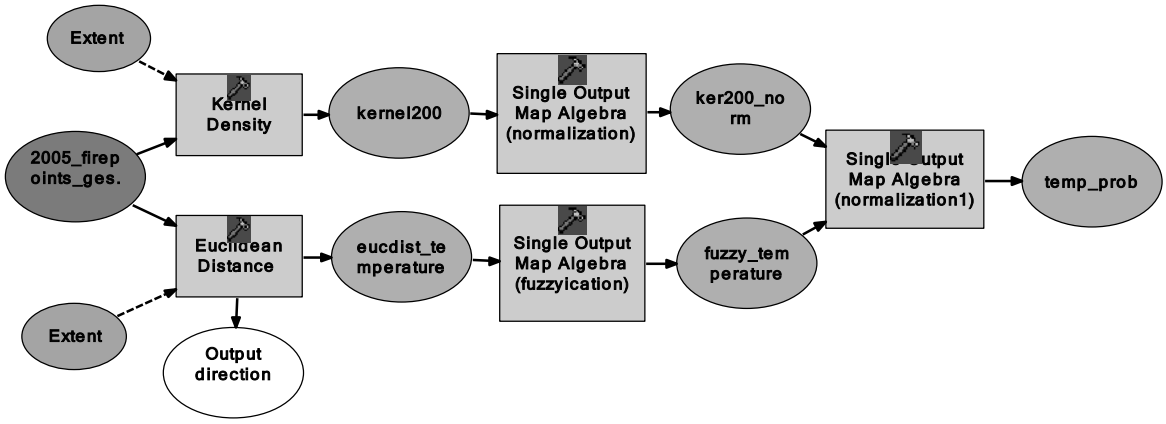

Figure 5.5: Flow scheme for probability map generation from temperature data in ModelBuilder

Thermal anomalies

Thermal anomalies in the LS7 data result from energy flux to the surface induced by the subsurface fire source. However, other sources account for thermal anomalies, too. Of these non fire sources, solar heating and water surface effects can be quite efficiently reduced through employment of night time data and filtering (ZHANG, 2004). Not every non fire induced anomaly can be removed, however. This is especially true for urban or industrial heat sources which tend to display geometric properties similar to the one of a coal fire. Both constitute rather punctual sources with high heat concentration (e.g. industrial chimneys). Because of this ambiguity thermal anomalies were regarded as class 2 indicator for the hypothesis „fire“ with a basic probability mass of 0.5.

Field studies on coal fires showed that anomalies produced by coal fires are mainly expressed as hot exhaust gas emissions at cracks (ZHANG, 2004). They commonly do not exceed some few meters distance from the crack, meaning that anomalies commonly cover sub pixel area on medium resolution satellite imagery. Yet, an anomaly with sub pixel area can theoretically only be detected if its temperature is large enough to raise the average temperature of the pixel above the detection threshold

of the sensor. This threshold is given by the sensor's radiometric resolution, which can then be converted into a threshold temperature difference (VAN GENDEREN & GUAN, 1997). For LS7 data it has been demonstrated that for an anomaly to be detected a temperature of 438 K (165 °C) and an area of 40 m² is necessary (ZHANG, 2004). Considering that during field campaigns anomalies were found to be rather small area implies that

- anomalous pixels tend to represent very hot heat sources resulting from fires covering a much larger area underground and therefore
- anomalous pixels tend to underestimate the real fire extent.

Moreover anomalies consisting of more than one pixel were assumed to be caused by one coherent fire area. Accordingly, the interior of the anomaly clusters was assigned a constant probability value of 0.5 on the probability map. Around the clusters a transition zone of 60 m corresponding to the size of one LS7 pixel with linear decreasing probability was generated to account for possible underestimation of the fire extent.

Probability map generation for the thermal anomalies was based on Euclidean distance to the thermal anomaly clusters. The distance raster was converted into a probability raster through map algebra according to the conditions:

- for distance = 0 assign constant value of 0.5;
- for 0 < distance < = 60 assign (distance - 60) / (-120);
- for distance > 60 assign constant value of 0.

Longwall mining

The goafs represent areas of high ignition risk. The longwall mining technique used in the Wuda Syncline leaves a solid layer of coal on the bottom of the exploited panels (GIELISCH, 2004), supplying the fuel for coal fires. Leftover coal debris from mechanical machining of the seam is especially prone to self ignition due to the small particle size and the corresponding high surface area (WALKER, 1999). Cracks developing attendant to subsidence serve as vents for the circulation of air thus accelerating spontaneous combustion. In summary, conditions for self ignition of coal in the goafs are ideal. Despite this, presence of goafs rather represents a fire risk indicator

than a direct fire indicator, the goafs were therefore classified as class 3 indicator with a basic probability mass of 0.25 for the hypothesis „fire“.

The area covered by the goafs was assigned a constant probability of 0.25. Around the goafs, a transition zone of 100 m with linear decreasing probability allows for the fact that fires might have spread to the surrounding unmined seam. Given a maximum propagation speed of a fire front of 40 m yr^{-1}, (WESSLING, LEIBNITZ INSTITUTE FOR APPLIED GEOSCIENCE 2005 PERS. COMM.) the transition zone allows for a two and a half years long undetected spreading of a fire.

The probability map was generated from the Euclidean distance to the mapped goafs using the below conditions:

- for distance = 0 assign constant value of 0.25;
- for 0 < distance < = 100 assign (distance - 100) / (- 400);
- for distance > 100 assign constant value of 0.

Mining Activity

Mining activity is the prime precondition for underground coal fires in Wuda. It was discussed that inadequate mining techniques leaving solid coal and coal debris promote spontaneous combustion. In addition poorly sealed mine openings and ventilation shafts allow air circulation accelerating the self heating process and providing oxygen supply for the fire. Especially where information on the exact extent and location of the mined area underground is missing (which is the case for the private operated mining) mining activity features give a hint for enhanced fire probability. Since the mining activity data has to be considered as a risk factor rather than a concrete fire indicator, it was classified as a class 3 indicator and assigned a basic probability for the hypothesis „fire“ of 0.25.

Most mining related surface infrastructure is located in close vicinity of the coal outcrops. The risk emanating from these features can only proceed in dip direction of the seams, since the fire can only burn into the seam. The zone of enhanced fire probability can only extend in the same direction. The probability for a fire emanating from a mining activity feature was assigned a constant value of 0.25 within a 100 m radius. Outside this buffer the probability decreases to zero within another 100 m, which is indicated by a linear fuzzy transition zone. Both zones only stretch into the dip direction of the coal seam. A radius of 100 m takes into account the common inability to

determine the exact position of the mining activities (e.g. the mine entrance or the cliff of the open cast mining). Moreover, the zones allow for subsurface features like mining tunnels departing from the entrance, which are not visible in the satellite data.

In deriving the probability maps from mining features it had to be ensured that probability only propagates in direction of coal seams. To allow for asymmetrical propagation of distance the Cost Distance Function of Spatial Analyst (see appendix for details on this function) was used. The cost raster was generated manually by digitizing the outline of the outermost coal seam. The boundary polygon was then converted into a raster with the Feature to Raster Conversion Tool (see section 6.1.2 for details on this function) in the ArcToolbox. Because of the synclinal structure, the coal seams show centroclinal strike, which means that the seams extend towards the middle of the ear shaped syncline. The outermost seam then also outlines the boundary of the coal deposits. The raster obtained from the boundary polygon was reclassified using the Reclassify Function of Spatial Analyst with the interior of the syncline assigned low cost weight and the outside high cost weight to form the cost raster used in cost distance analysis. The resulting cost distance raster was finally converted into a probability map using the following conditions:

- for distance < = 100 assign constant value of 0.25;
- for 100 < distance < = 200 assign result of (distance - 200) / (- 400);
- for distance > = 200 assign constant value of 0.

Coal deposits

Subsurface coal fires can only occur inside coal seams. Therefore, where the presence of coal deposits can be excluded, a zero probability for a coal fire can be assumed. Conversely, the presence of coal seams doesn't imply the presence of a coal fire. Consequently, the distribution of coal was used as a class one indicator for the hypothesis „no fire". Notably this implies a basic probability of one for this hypothesis being true where coal deposits are absent.

Determining the area of the coal deposits with the possibility to host coal fires involved three constants in addition to the mapped coal seam outcrops:

- the strike which shows the centroclinal direction of a fold (GIELISCH, 2004)

- the fall (dip angle) of the seams which varies between 5 and 30° (GIELISCH, 2004)
- the maximum depth of 150 m coal fires can reach due to limited oxygen supply (JIA & SUN IN KÜNZER, 2005).

The maximum horizontal distance (z) from the seam outcrops where fires can occur are obtained by

$$z = \frac{MAX(firedepth)}{\tan(dipangle)} \qquad \text{(Eq. 19)}$$

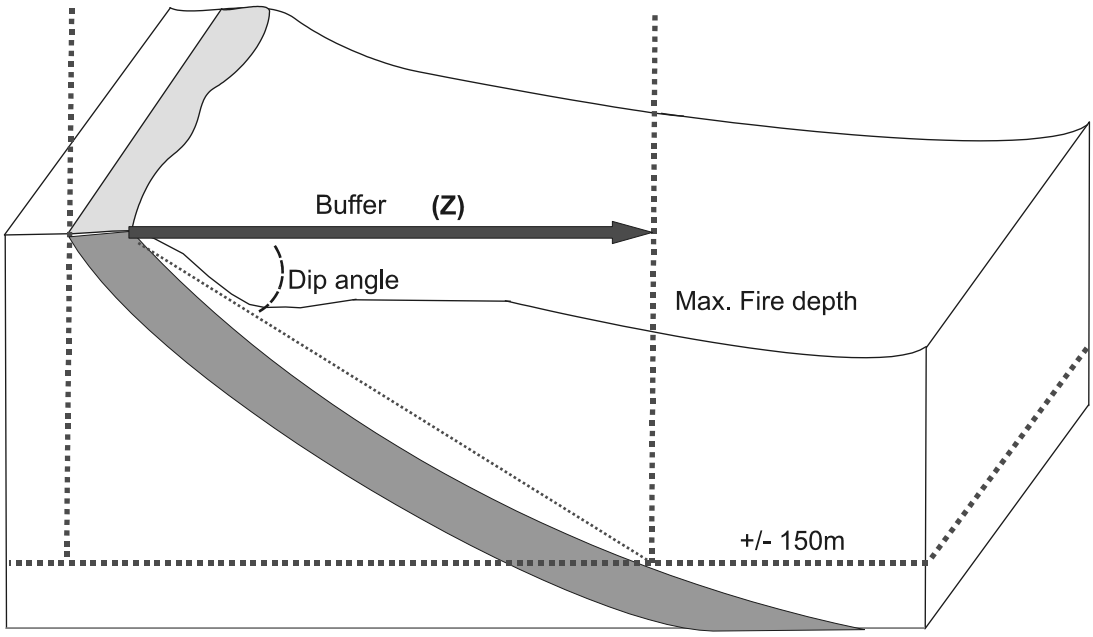

Figure 5.6: B**uffer zone around coal seam outcrops**

It was assumed that starting from a depth of 75 m fires are increasingly unlikely. Thus, a buffer zone of 850 m corresponding to a minimum dip angle of 5° and a depth of 75 m was created around the seam outcrops with a zero belief in the hypothesis „no fire“. Adjacent to the buffer lies a transition zone with increasing belief in the hypothesis „no fire“ reaching a value of 1 at the distance of 1700 m corresponding to a minimum dip angle of 5° and a depth of 150 m.

The same cost distance function already used for the mine activity data was employed to generate the distance raster. By applying the conditions given below the cost distances were then converted into probabilities.

- for distance < = 850 assign constant value of 0;

- for 850 < distance < = 1700 assign result of (distance – 850) / 850;
- for distance > 1700 assign constant value of 1.

Table 5.2 sums up the indicators and the constraints limiting their prediction value for the given hypothesis.

Table 5.2: Evaluation of indicators with respect to their prediction value for coal fires

Indicator	Constraints
Temperature measurements	enhanced surface temperatures prove the existence of a subsurface fire but give only limited hint about the actual fire location
Thermal anomalies	Thermal anomalies in LS7 data can have other causes than a fire Not every fire produces a thermal anomaly in LS7 data
Cracks	Cracks can also be caused by underground mining Not every subsurface fire produces cracks
Longwall mining	Subsurface fires often occur in the goafs, but they do not inevitably have to occur there
Mining activity	Most subsurface fires occur in the wake of mining activity, but mining activity doesn't inevitably trigger fires
Coal seams	subsurface fires can only occur in coal seams

5.4 Combining the evidence

The probability maps expressing the evidence from the respective indicators were then combined according to Dempster's original combination rule (equation 12). The orthogonal sum honours the rule that the sum of all BPAs must equal one anytime (LORUP, 1999). Only two maps can be combined at a time, additional maps are combined with the higher aggregated results in successive steps. The order of combination doesn't play a role, since the combination rule is commutative (SHAFER, 1976). Table 5.3 illustrates the procedure of combining two probability maps supporting the hypothesis „fire". The assignable probability mass *m* per indicator is one. Hence, the remainder of *m* not assigned to the hypothesis „fire" has to be allocated to the frame of discernment Θ, which represents the inability to make a decision for either of the hypotheses. The orthogonal sum implies successive multiplication of focal elements

which are subsets of Θ associated with nonzero values of *m*. To obtain the aggregated mass for the hypothesis „fire“, all products with a non empty set for the intersection of the hypothesis under consideration were summed, which is hinted in the last row of table 5.3. Practically, the probability maps were multiplied and the multiplication results summed using map algebra with the (prototype) syntax:

```
support fire = [probability map A] * [probability map B] +
(1 - [probability map B]) * [probability map A]
+ (1 - [probability map A]) * [probability map B]
```
(Eq. 20)

To calculate the difference (1 - [probability map]) a constant raster with the value 1 was generated using the Create Constant Raster Tool of Spatial Analyst.

Table 5.3: Orthogonal summation of concurrent evidence. After (LORUP, 1999)

	Evidence A [fire]		
Evidence B[fire]	**Orthogonal sum ⊕**	**m[fire]**	**Θ = 1- m[fire]**
	m[fire]	[fire] · [fire] = A	Θ · [fire] = B
	Θ = 1- m[fire]	[fire] · Θ = C	Θ · Θ = D
	$M_{aggr}[fire] = A + B + C$		

In calculating the final belief in the hypothesis „fire“, the aggregated probability maps for the hypothesis „fire“ had to be combined with the probability map for the hypothesis „no fire“ resulting from coal distribution data. These two probability maps represent conflicting evidence, therefore normalization according to equation 12 was needed. Computation of the resulting belief map is illustrated in table 5.4.

Table 5.4: Orthogonal summation of conflicting evidence. After (LORUP, 1999)

	Evidence A [fire]		
Evidence B [nofire]	**Orthogonal sum ⊕**	**M[fire]**	**Θ = 1- m[fire]**
	M[nofire]	[fire] · [nofire] = A	Θ · [nofire] = B
	Θ = 1- m[nofire]	[fire] · Θ = C	Θ · Θ = D
	Belief[fire] = C/(1-A) *Belief[nofire] = B/(1-A)*		

The general map algebra syntax was:

```
belief fire = (1 – [coal probability map]) *
[final probability map fire] / (1 – [coal probability map] *
[final probability map fire])                                    (Eq. 21)
```

The denominator in equation 27 the term after the minus is k, the degree of conflict.

Generating the final belief map for the hypothesis „no fire“ required combining the aggregated probability map for the hypothesis „fire“ and the probability map for the hypothesis „no fire“. According to the last row of table 5.4 computation employed the map algebra syntax:

```
Belief nofire = (1 – [final probability map fire]) *
[coal probability map] / (1 – [coal probability map] *
[final probability map fire])                                    (Eq. 22)
```

The plausibility and belief interval maps were then calculated according to equations 9 and 10. The syntaxes can be viewed in table A.1 in the appendix and are not listed here. Figure 5.7 sums up the work flow for Dempster- Shafer analysis within this thesis.

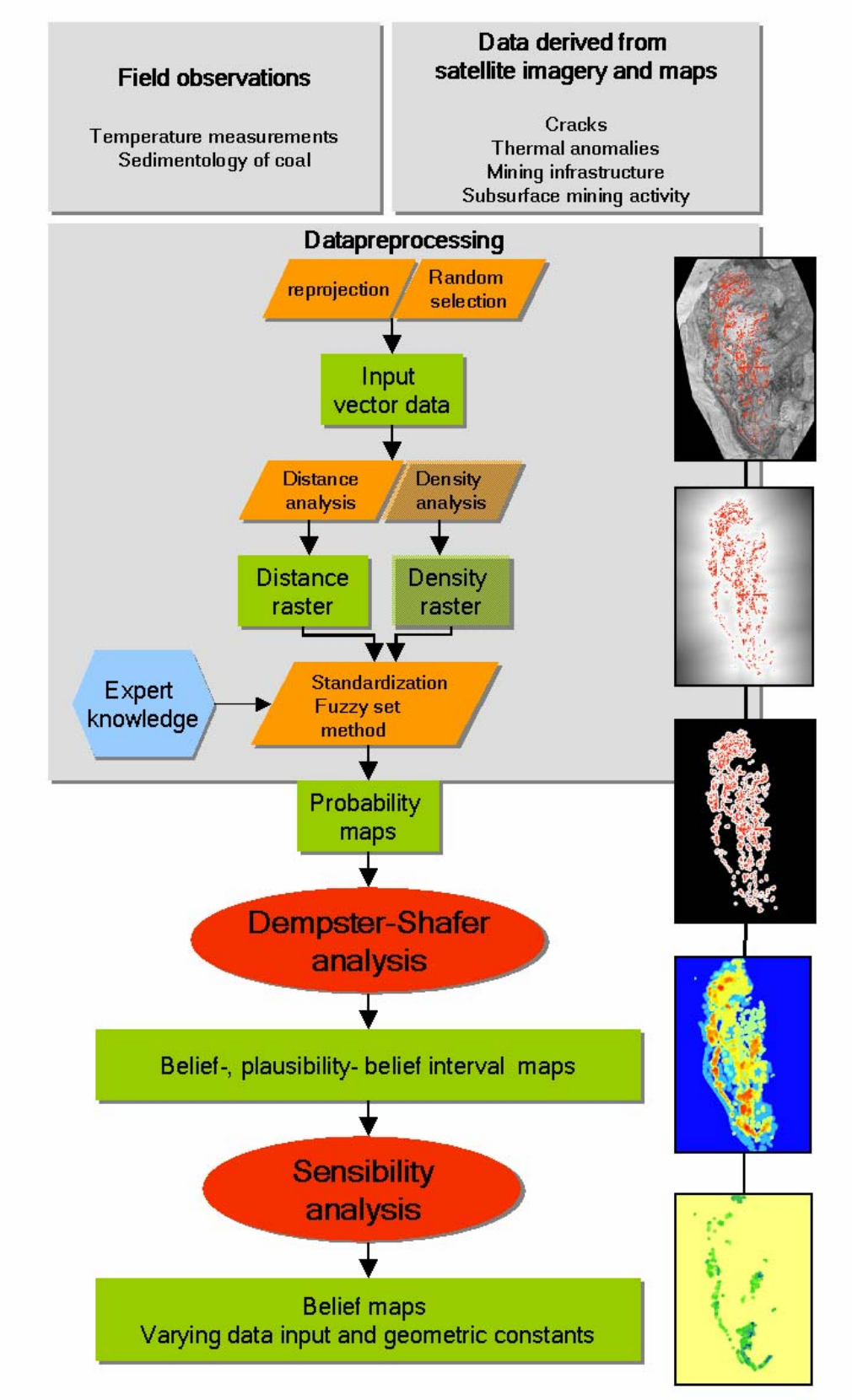

Figure 5.7: Flow model for implementing Dempster-Shafer Analysis

5.5 Vector versus raster format

In general, two types of data models are distinguished for representing spatial data in GIS: vector and raster. Data sets in vector format are entities represented by multiple pairs of coordinates while one coordinate tuple/triple represents one point. By connecting points, lines can be generated, thus a line in vector format is represented by a number of coordinate tuples/triples along its length. Polygons can be generated by connecting the line back to the starting point. A set of coordinates at the corners of the polygon defines its spatial component. In the geo relational model each of the objects of a vector layer has a unique identifier which points to its attributes stored in an attached table. In the geodatabase model objects are stored as rows of a table containing their spatial and thematic attributes. The objects stored in vector format have a definite spatial relation denoted as topology, which allows spatial analysis on geographical data.

Data sets in raster format are stored in a two-dimensional matrix of uniform grid cells or pixels. These pixels are usually square or at least rectangular. In the raster data structure the only topology is cell adjacency. The value of each pixel represents the thematic information at a given location. Due to the fact that each pixel represents only one value, the resolution of the provided information depends on the cell size of the raster image.

The vector model undoubtedly has its strength in representing discrete real world objects. For representing continuous phenomena such as elevation or distance, the raster model is commonly chosen. The probabilities as well as beliefs and plausibilities of Dempster-Shafer are a continuous phenomenon, for they are functions of the distance to the features indicating a hypothesis. Therefore, a raster based approach was considered most suitable for generating fire probability-, belief, plausibility and belief interval maps.

5.6 Handling multi source and resolution data

The incorporated data was derived from sources with different scale and spatial resolution (table 5.5). For the satellite data the spatial resolution, which is the sensor resolution, as well as the geometric accuracy can be estimated. The latter is derived from the Root Mean Square Error (RSME) during geometric image correction. For the map derived data the spatial resolution was approximated by the scan resolution. The spatial resolution of the field data was estimated based on the geometric accuracy of the used GPS.

Table 5.5: Metadata for the indicators used in this thesis

Dataset	Source	Spatial Resolution/	Geometric accuracy	Date
Temperature measurements	Handheld infrared radiometer georeferencing by GPS		10 – 20 m	2005
Thermal anomalies	Landsat 7 ETM+ TIR band	60 m	< 30 m	2003
Cracks	Quickbird panchromatic channel	0.6 m	< 2 m	2003
Mining Activity	Quickbird panchromatic channel	0.6 m	< 2m	2003
Longwall mining activity	Analogue map 1: 10000	~1 m	unknown	~ 2000
Coal seams	Analog map 1: 10000	~1 m	unknown	~ 1980
Known fire areas	Synthesis from spatial photography, temperature measurements and borehole drillings georeferencing by GPS		10 – 20 m	2004

Geological and mining maps were available as photocopies from the original maps in 1: 10000 scale. Given a scan resolution of 300 dpi the resolution of the fotocopy can be estimated by

$$10000 \text{ cm} / (300 \text{ lines} / 2.54 \text{ cm}) = 0.85 \text{ m line}^{-1}$$

Thus the coal seam and longwall mining data can be assumed to have a spatial resolution of about 1 m. The pocket GPS used to georeference temperature measurements has a geometric accuracy of 10 m to 20 m given an advantageous geometric constellation of satellites (http://www.garmin.de/Produktbeschreibungen /iQue3600.php) (12.04.06). This was assumed to be the spatial resolution range for the surface temperature field data. The cracks and mining activity data as well as the thermal anomaly data have a resolution according to the sensor resolution of 0.6 and 60 m, respectively. The geometric accuracy was < 2 and < 30 m, respectively (KÜNZER, 2005)

The target resolution depends on both, the scale and resolution of the incorporated data and the application scale. For an application of the algorithm in the context of a regional to larger scale monitoring strategy a spatial resolution of 100 m would be reasonable for two reasons: first, satellite imagery is likely to constitute the only source to derive fire indicators from and second, probability maps with this resolution would be a sufficient basis for the coordination of fire extinguishing activities in the field. Once a fire is pinpointed in the field with an accuracy of around 100 m the exact location can quickly be determined by borehole drillings. More often, the fire can already be located by means of its physical signs at surface. However, in the at hand case study the extensive fine resolution data base and the local scale of the study area justify a fine target resolution. To demonstrate the capability of the algorithm to reproduce known fire areas in the study area a resolution of 10 m was considered a good compromise within the resolution range of the available data and sufficient to resolve the shape of all fires.

5.7 Spatial reference

Assigning one standardised geographical reference to a set of different data layers in a GIS is the precondition for establishing topology between features of the different layers. This in turn is the basis for all inter - layer spatial analysis. As reference for all input, intermediate and output data, the Quickbird scene of the study area was chosen.
The projection parameters are:

Coordinate system:	WGS_84_UTM_Zone_48_North
False easting:	500000

False northing:	0
Central meridian:	105
Scale_Factor:	0.9996
Latitude of origin:	0
Datum:	D_WGS_1984
Linear unit:	1 meter

The input shape files were projected manually using the Feature Projection tool in the Arc Toolbox. The output raster maps were assigned the coordinate system specified in the input dialog of the application.

5.8 Summary

It was demonstrated that determination of coal fire probability can be viewed as a decision problem that can be effectively handled by the logic of DST. Based on general considerations on uncertainty modelling in spatial data, the procedure of transferring DST to coal fire probability modelling was described. First the frame of discernment was defined, which consisted of the hypotheses “fire” and “no fire”. Basic probabilities were then assigned to the datasets in a knowledge-driven approach considering the degree to which the indicator points to the supported hypothesis. Third, probability maps were generated for the datasets incorporating expert knowledge on the geometric relationship between the evidence features and the fire front. Finally, probability maps were combined according to Dempster’s rule. The output maps were assigned a cell size of 10 m and projected in UTM WGS 84 coordinates.

6. Implementation

The Dempster-Shafer algorithm was implemented in an integrated ESRI ArcGIS and Visual Basic .NET (VB.NET) environment. It was distributed as standalone executable to be run in an ArcGIS 9.x / Windows XP environment.

6.1 Software used

6.1.1 ArcGIS™ 9.1 Spatial Analyst

Software ArcGIS 9.1 of ESRI was used as GIS environment since this is the standard GIS software at DFD. LORUP (1999) has already demonstrated the potential of the predecessor software, ArcView GIS, to model DS beliefs and plausibilities. ArcGIS offers a rich set of tools to compile, author, analyze, map and visualize information with spatial reference.

The Spatial Analyst extension for ArcGIS is designed to perform spatial operations on raster data sets. It can be accessed via loading the extension into the ArcMap menu or via the Arc Toolbox Spatial Analyst functions. The main functions integrated in the application are described below.

Euclidean Distance Analysis

The Euclidean distance function calculates the distance from each cell in the raster to the closest source. The output raster cells are assigned the value of this calculated straight line distance in projection units of the raster to the closest specified source. Both, raster and vector files are accepted as source files. The distance is measured from cell centre to cell centre.

Cost Distance Analysis

The cost distance function is similar to Euclidean distance function, but instead of calculating the actual distance from one point to another, the cost functions determine the shortest weighted distance (or accumulated travel cost) from each cell to the nearest member in the set of source cells or features. The weighted distance functions use cost units instead of geographic units. Two input parameters are required: the cost raster provides the weight values for the raster cells; the source file provides the raster cells or

features constituting the source. On the output raster each cell is assigned the accumulative cost to the closest source cell or feature. For a detailed description of the algorithm the reader is referred to the ArcGIS Desktop help.

Kernel density analysis

Kernel density calculates the density of features in a circular neighbourhood of defined radius around each output raster cell. Conceptually, the kernel density function fits a smoothly curved surface over each feature. The surface value is highest at the location of the feature, and diminishes with increasing distance from the feature, reaching 0 at the search radius distance from the feature. The volume under the surface equals the population field value for the feature, or 1 if no population field is specified. The bigger the search radius the smoother the kernel density surface, for the field value for each feature is spread over a wider area. The density at each output raster cell is calculated by adding the values of all the kernel surfaces where they overlay the raster cell centre. Kernel density analysis can be operated on both, point and line features.

Map Algebra Analysis

Map Algebra is the language to perform mathematical operations, conditional statements, and local, focal, zonal, global, and application functions on raster data. The building blocks for the Map Algebra language are objects, actions, and qualifiers on the actions. Objects either store information or are values. They are inputs for computation or can be storage locations for output. Actions that can be performed on input objects are operators and functions. Operators perform mathematical computations within and between input objects. The set of operators is composed of arithmetical, relational, boolean, bitwise, logical operators and combinatorial operators. Functions allow for analysis in different spatial domains. Local functions pertain to a single raster cell and include e.g. trigonometric, algebraic or statistical functions. Focal functions manipulate the value of a raster cell dependent on the values of a defined neighbourhood. Zonal functions perform analysis on disjunctive raster cells with defined common value. Global functions calculate values for a raster cell based on full raster context. Euclidean distance is an example for a global function. Application functions are developed for specific tasks such as hydrologic modelling. Qualifiers are parameters that control how and where an action is to take place. A detailed description of the map algebra functionality can by found in the ArcGIS desktop help.

The Spatial Analyst functions described were incorporated in the code by referencing ESRI ArcObjects libraries.

6.1.2 ArcObjects ™

ArcObjects is the development platform for the ArcGIS familiy of applications. It is based on Microsoft Component Object Model (COM) technology. ArcGIS geoprocessing functionality can be accessed and integrated into any COM-compliant programming software.

Geoprocessing functionality provided by ArcObjects was used as building blocks of the Dempster-Shafer analysis tool developed in this thesis.

6.1.3 Visual Basic 2005 Express Edition ™ and Visual Basic .NET

Visual Basic 2005 Express Edition is the latest release of Microsoft's programming environment for the programming language VB.NET. VB.NET has evolved from its predecessor Visual Basic to obtain full object orientation. It is now one of the languages supported by the Microsoft .NET framework. The .NET framework 2.0 is the implementation of the Common Language Infrastructure standard by Microsoft. It consists of a runtime environment (the Common Language Runtime CLR) and a set of class libraries (the Framework Class Library). The CLR is capable of compiling and executing code written in different languages, such as C++, C# and Java.

A free trial version of Visual Basic 2005 Express Edition was used to write code implementing the Dempster-Shafer algorithm.

6.2 Description of the Dempster-Shafer analysis tool

The tool performs Dempster-Shafer belief modelling on specified input data. In a simple graphical interface the user is asked to specify the data sets to be incorporated in the analysis by providing their file names and paths. Only ESRI Shape format is accepted. Crack and anomaly data are mandatory input. Any of the other data sets are

optional. Moreover, the user is asked to specify the output extent, the output projection and the output directory.

The assignment to one of the two hypotheses “fire” or “no fire” as well as the respective basic probability mass is preassigned in the code. However, the user can change the geometry of the probability distribution in a configuration file in .txt format containing the diameters of the buffer and transition zones and the output cell size in a defined order.

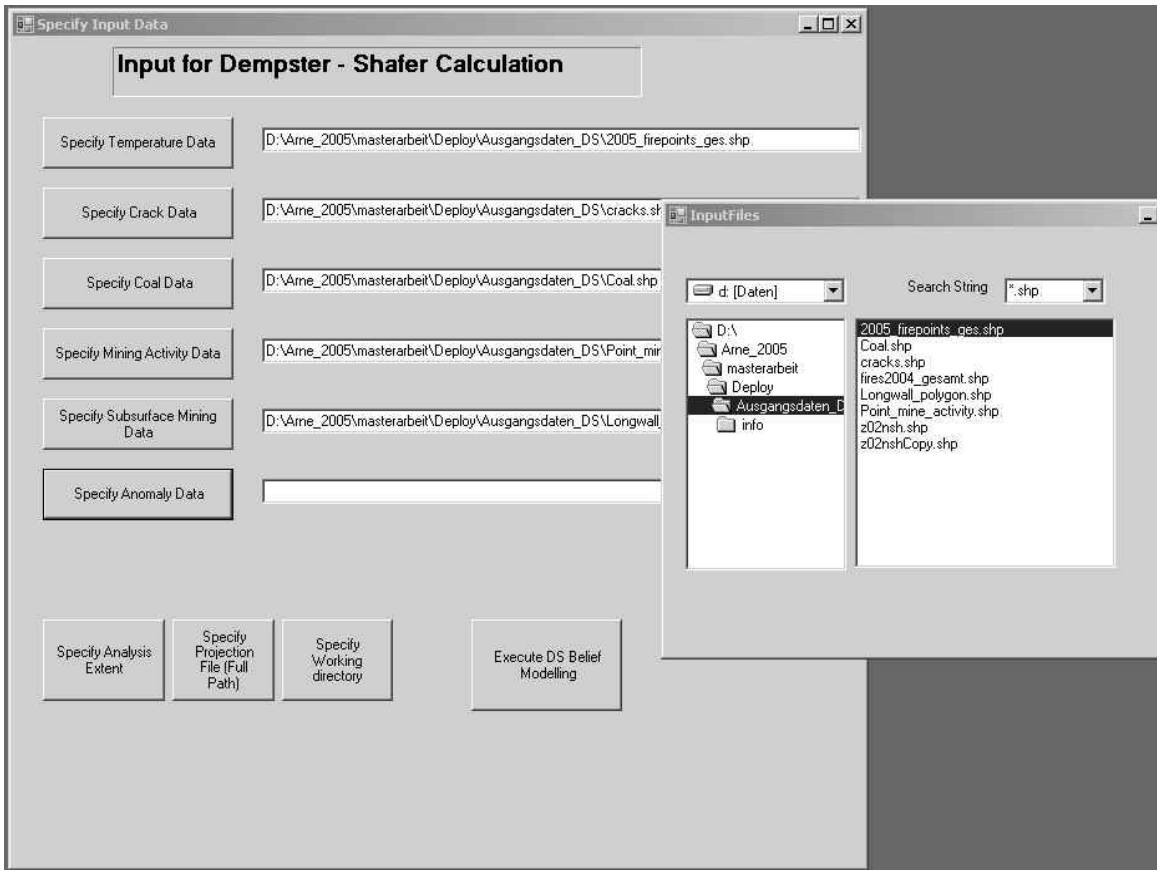

Figure 6.1: Graphical user interface

The application is structured into form modules, controller modules and a function module. The form modules collect the input information. The controller modules test for the input made by the user and determine the program flow accordingly. The function module performs distance analysis, map algebra operations, raster creation and data management operations. Its functions are called from the form or controller modules passing in specific variables. Thus modularity of the code is assured. Table A.1in the appendix lists the core spatial analyst functions. Data management functions include check for availability of Spatial Analyst licence, conversion to permanent raster

files and an overwriting function in case a file with the specified name already exists in the directory.

All intermediate files that is the distance-, probability-, belief-, plausibility- and belief interval maps are written to the specified output directory. Figure 6.2 resumes the basic program flow.

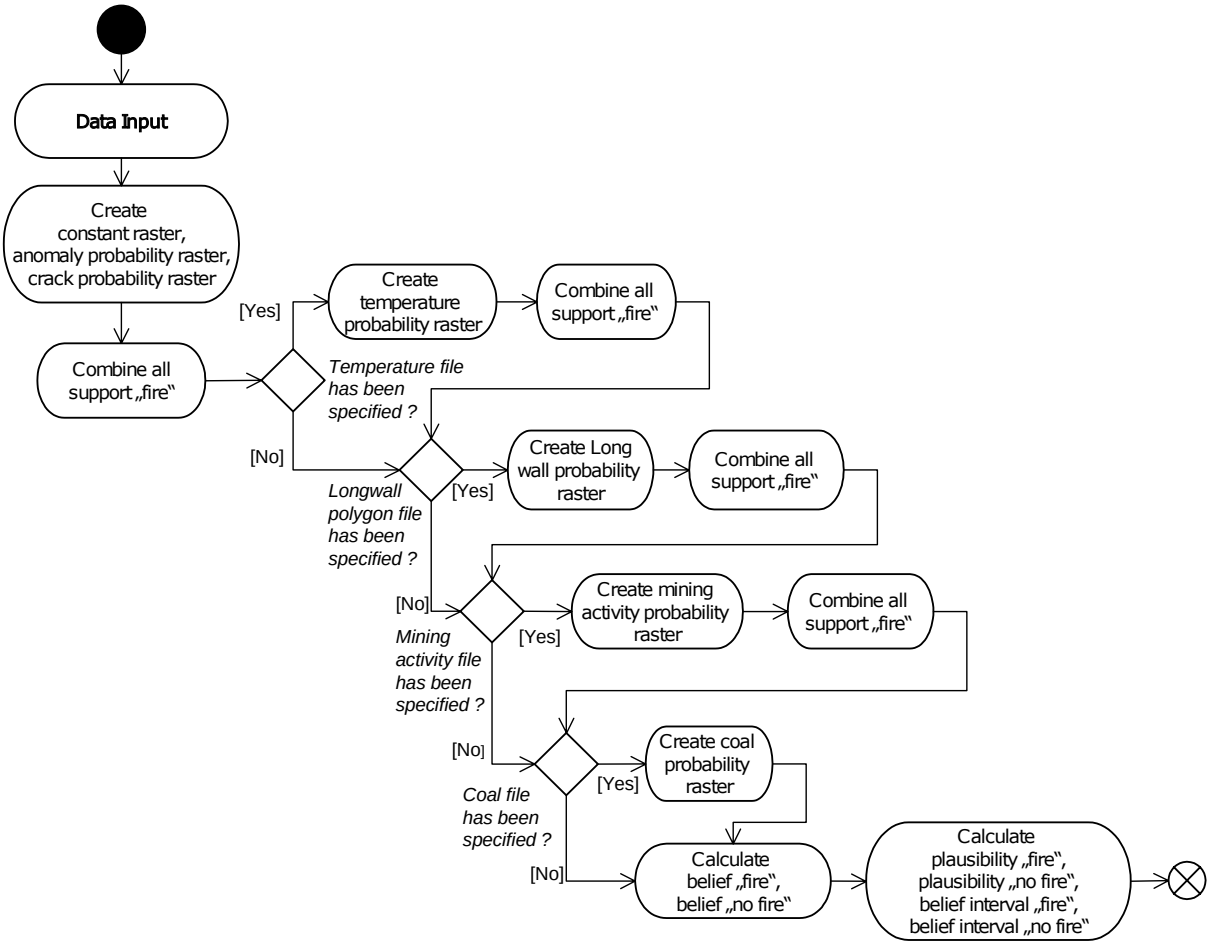

Figure 6.2: Program flow in UML notation

6.3 Summary

ArcGIS 9.1 was used as GIS environment to implement raster based DS belief modelling. Spatial Analyst, an extension for ArcMap provided raster based geoprocessing functionality incorporated in code development. The functions were embedded into the code by referencing the respective ArcObjects 9.1 components. The code was written in VB.NET using the Visual Basic 2005 Express Edition developing environment.

The application generates probability maps from fire indicators specified by the user, as well as belief-, plausibility and belief interval maps for the hypotheses “fire” and “no fire”. The resulting maps are written out as ESRI grids.

7. Results and discussion

7.1 Probability maps

Figure 7.1 shows the probability maps for the 6 selected indicators. Increasing probability for the respective hypothesis to be true is visualized through increasingly dark colour. The respective input feature data is superimposed to demonstrate the geometry of the probability function. On the maps supporting the hypothesis “fire” (figures 7.1 A to D and F) probability is decreasing with increasing distance from the features. On the map derived from coal seam distribution probability increases with distance, since this data set is supporting the hypothesis “no fire” (Figure 7.1 E).

A closer look on the probability map generated from field temperature measurement (detail frame in Figure 7.1 B) reveals the effect of the kernel density function. The initial buffer is marked by the medium grey zone with constant diameter. Within this zone, darker areas mark higher probability for a fire as suggested by clusters of high values in the temperature data. Zones of brighter grey values mark lower probability corresponding to lower magnitude for the measured temperature.

The detail frames in figures 7.1 E and F highlight the effect of the cost distance function. Since the boundary of the coal deposits is outlined by the outermost coal seam outcrop, the probability for the hypothesis „no fire“ provided by the coal seam distribution increases within short distance outside this seam (Figure 7.1 E detail frame). In contrast, in direction of the strike, the buffer and transition zones are much broader. The same is true also for the mining activity features. A major part of mining activity is found along the outcropping seams. Fire probability emanating from these features also abruptly decreases outside the outermost outcropping seam (Figure 7.1 F detail frame).

Comparison with the mapped coal fires (Figure 7.1 G) shows that except for the field temperature measurements, the single indicators do not reflect location and extent of the fire zones in the study area.

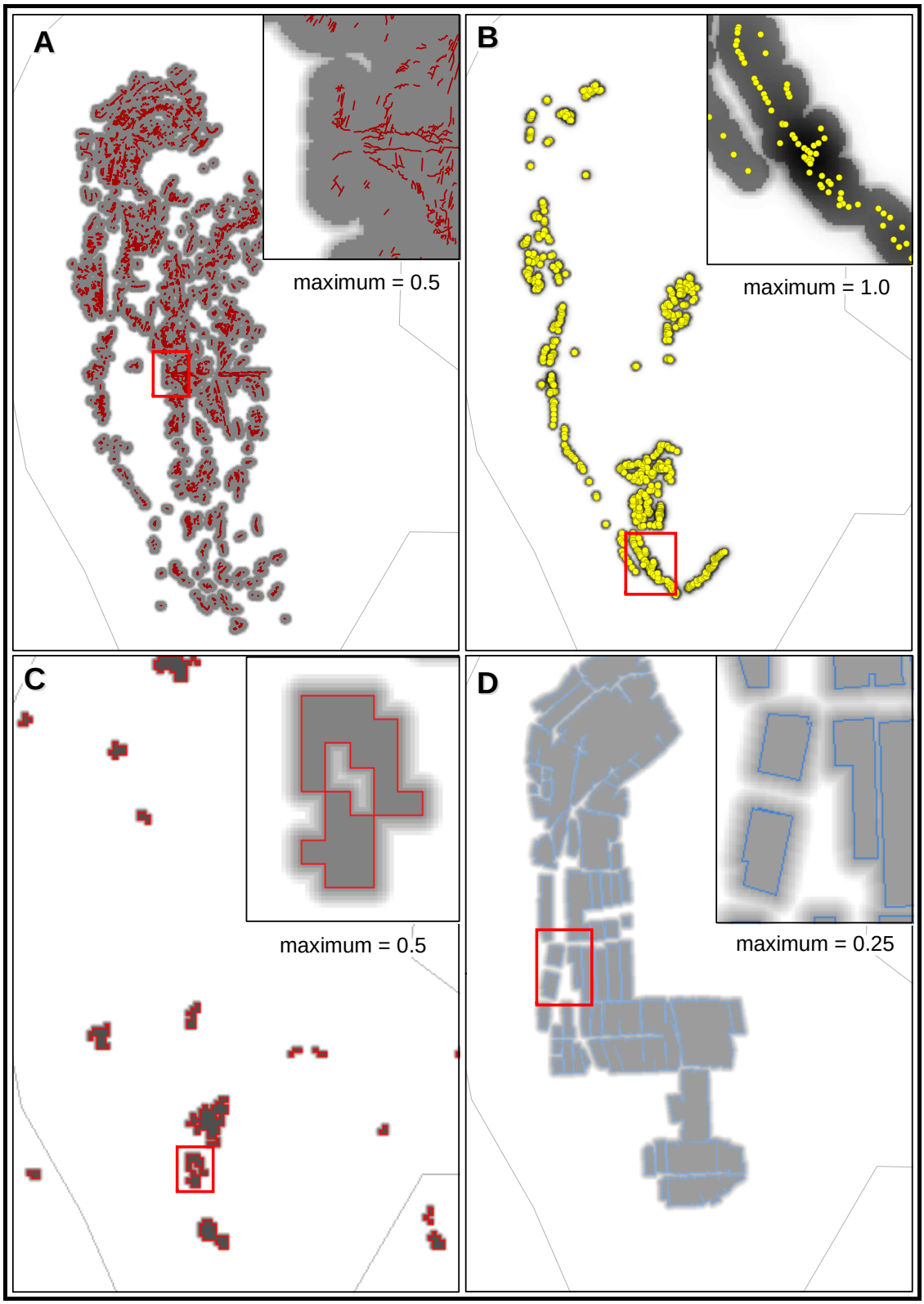
A
maximum = 0.5
B
maximum = 1.0
C
maximum = 0.5
D
maximum = 0.25

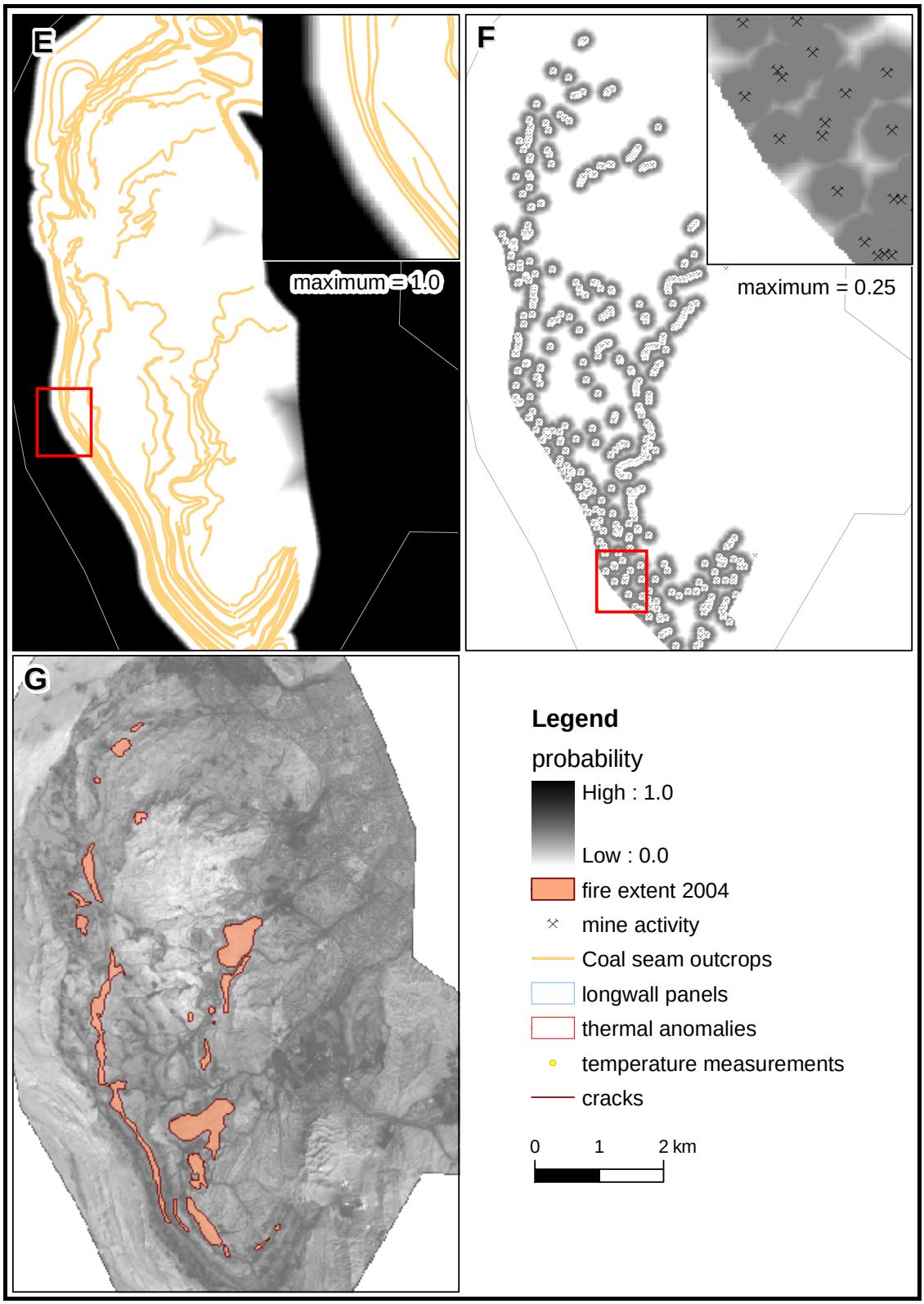

Figure 7.1 : Probability maps derived from crack data (A), field temperature measurements (B), thermal anomalies (C), longwall mining data (D), coal seam distribution (E) and mine activity data (F). Location of known fires 2004 (G)

7.2 Dempster-Shafer analysis results

In the following section the results of DS analysis are presented. It was discussed in chapter 3.2.1 that Dempster's original combination rule is known to yield unexpected results in the case of highly conflicting evidence. When the degree of conflict converges to one, the term (1 - k) in the denominator of equation 12 converges to zero and the orthogonal sum doesn't exist. Figure 7.2 shows the distribution of k. It is obvious that conflict only occurs outside the syncline as a result of contradictory evidence from coal and thermal anomaly data. On one hand absence of coal deposits within 150 m below top ground surface strongly suggest rejection of the hypothesis „fire", on the other hand occurrence of thermal anomalies implies a contradictory probability that this hypothesis might be true. In this case contradiction is presumably due to anthropogenic heat sources causing the thermal anomalies in the TIR Band of LS7.

However, in a two hypotheses decision problem under the assumption of ignorance, Dempster's rule yields reasonable results in any but the case of complete contradiction. This is demonstrated in table 7.1, which shows the result for belief in the hypotheses "fire" and "no fire" for various hypothetic conflict situations. The conflicting belief masses for a given raster cell are found in the outer row and column. The complement to 1 is assigned to the frame of discernment (not shown). The inner rows and columns give the results with the belief "no fire" in the upper right and the belief "fire" in the lower left of each field.

Table 7.1: Results for belief in both hypotheses under various degrees of conflict

Bel(No Fire) / ***Bel(Fire)***		***m(no fire)***			
		0,5	0,9	0,99	**1,0**
m(fire)	0,5	**0,333** **0,333**	**0,818** **0,091**	**0,980** **0,010**	1 0
	0,9	**0,091** **0,818**	**0,474** **0,474**	**0,908** **0,083**	1 0
	0,99	**0,010** **0,980**	**0,083** **0,908**	**0,497** **0,497**	1 0
	1,0	0 1	0 1	0 1	Not def. Not def.

To conclude, Dempster's original combination rule will deliver reasonable results estimating coal fire probability for the degree of conflict within the data for the study area.

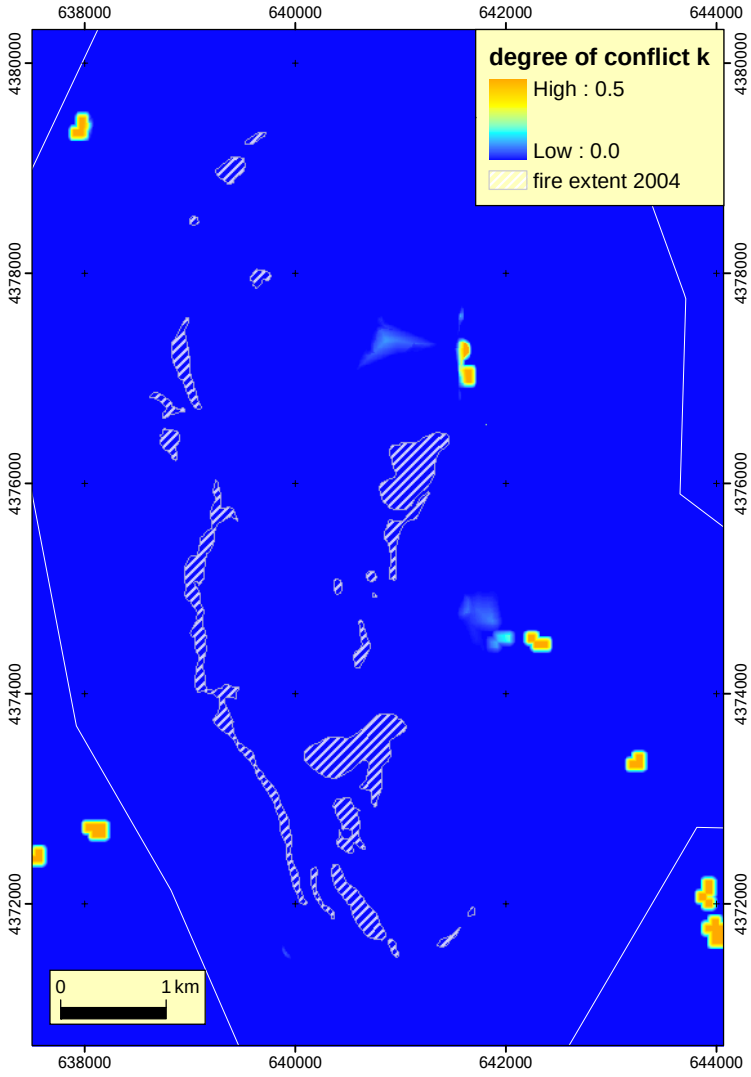

Figure 7.2: Degree of conflict in the study area

7.2.1 Belief in the hypothesis „fire"

All maps shown in the upcoming chapters are displayed using the same colour ramp and the stretch type "histogram equalize" to allow for comparability. Figure 7.3 shows the belief map for the hypothesis „fire". It was explained in section 3.1.3 that belief denotes the accumulated evidence for the hypothesis „fire". The map shows distinct zones of strong belief in the presence of a subsurface fire in good agreement with known fire locations. The year 2004 status of the fire extents is marked by red

polygons. Except for fire 10 each of the known fires is reflected as a zone of strong belief. More over, in the case of large area fires such as fires 7, 8, 11 and 12, the area is largely reproduced by the shape of the calculated local belief maxima. In particular, high belief magnitude is found in the vicinity of fires 3, 8, 11, 12, 18, which is in perfect agreement with findings from field visits in 2004 and 2005. Visible and sensible signs for intense fire activity were then reported for fires 11 and 12, the former of which was not accessible due to heat production and danger of collapse of the overburden (HIRNER, 2005 PERS. COMM.).

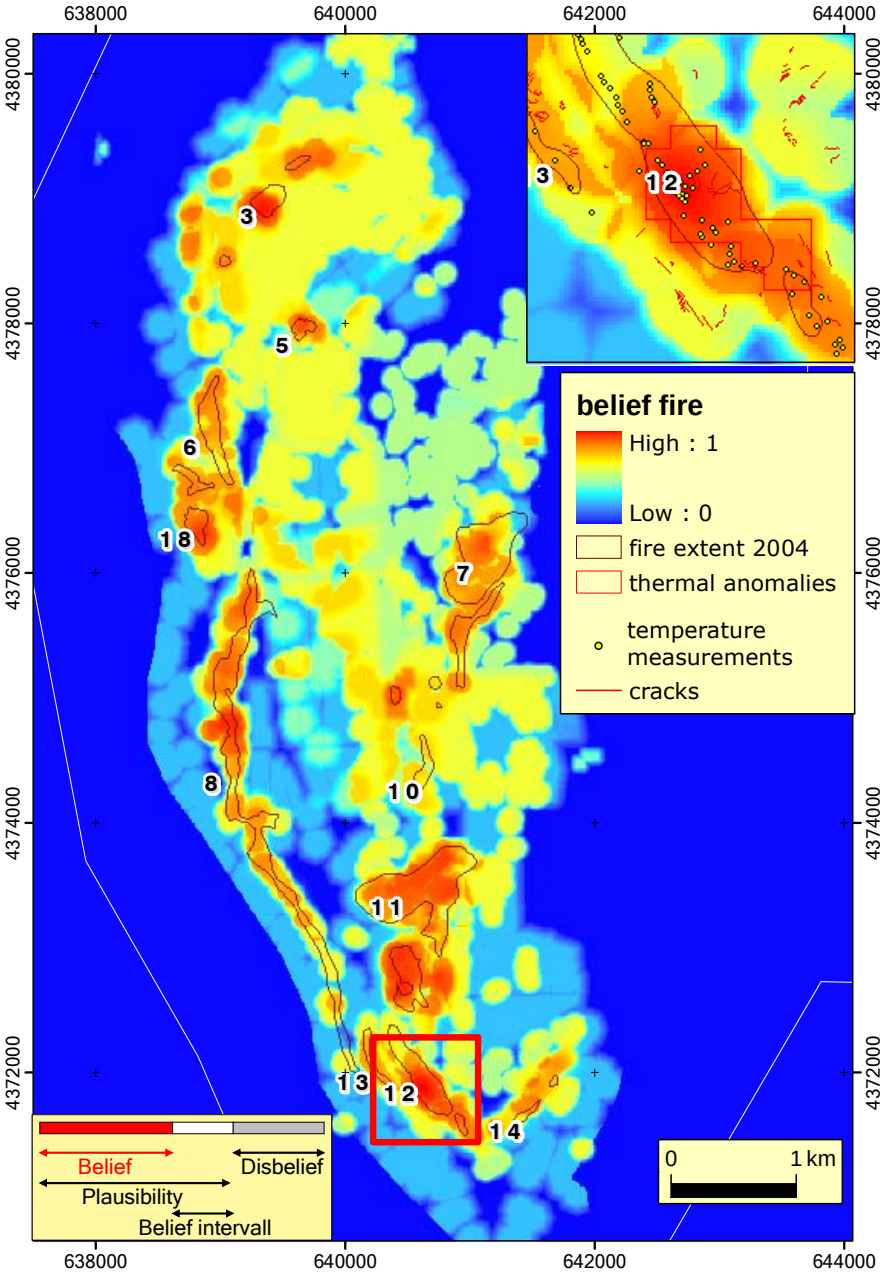

Figure 7.3: Belief map generated for the the hypothesis „fire“

The detail view of fire 12 illustrates the inherent character of the Dempster-Shafer rule of combination to reinforce belief in a hypothesis in the case of concurrent evidence. Here, evidence deriving from the presence of cracks, high surface temperatures and thermal anomaly expression in the LS7 TIR band each strongly indicate the presence of a subsurface fire. In the centre of the year 2004 outline of fire 12 they overlap to form a local “hot spot” of believe.

7.2.2 Belief in the hypothesis „no fire“

Since evidence for the hypotheses „fire“ and „no fire“ is spatially disjoint, combination of the conflicting pieces of evidence doesn’t modify the initial belief in the hypothesis „fire“ given by the coal distribution data. Hence, the belief map is identical with the probability map for the coal distribution data (figure 7.1 E), showing high belief outside the outermost outcropping seam of the syncline and zero belief in the interior of the syncline. The zero belief inside the syncline has to be interpreted as inability to make any statements concerning the absence of coal fires. Notably, this doesn’t automatically imply a high belief in the presence of a fire in this area.

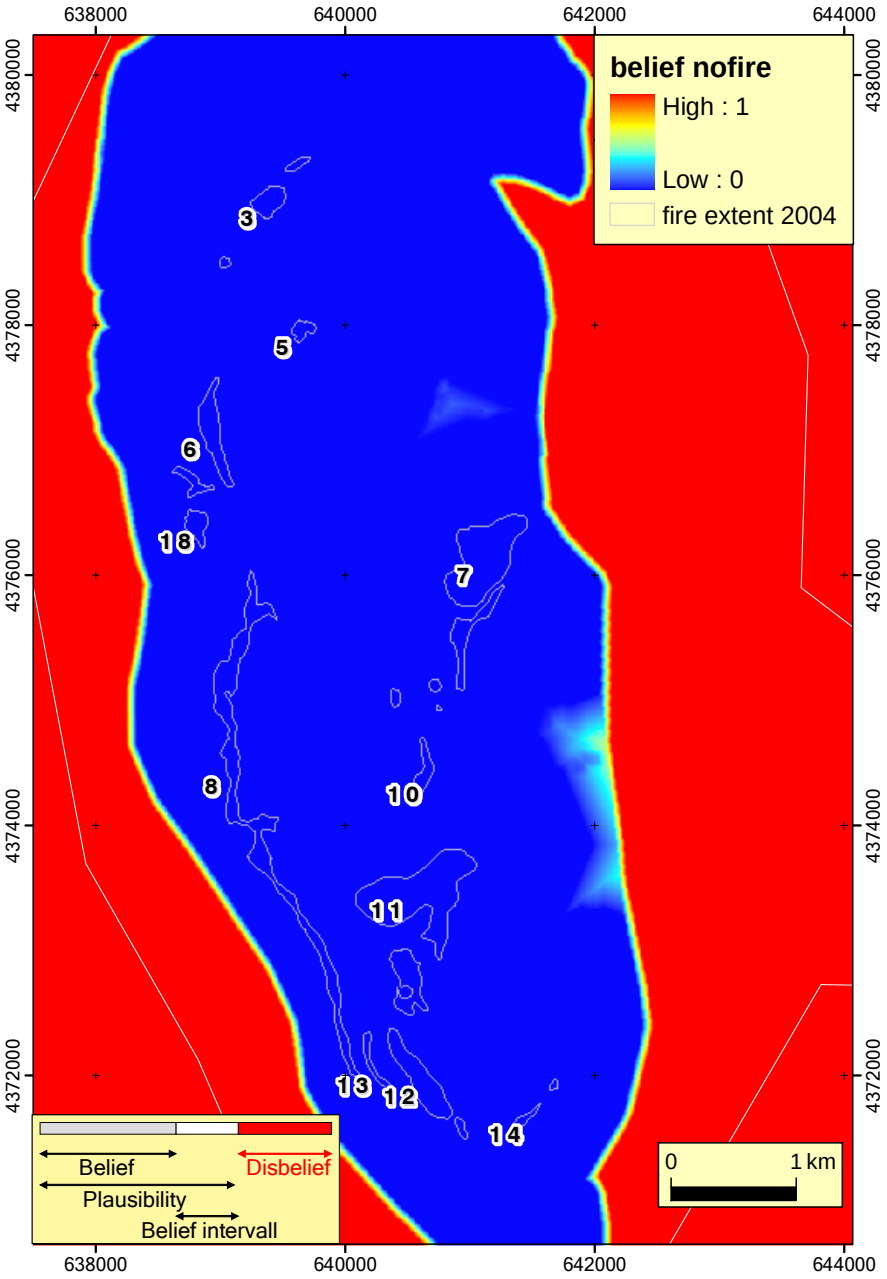

Figure 7.4: Belief map generated for the hypothesis „no fire“

7.2.3 Plausibility for the hypotheses „fire“ and „no fire“

Figures 7.5 and 7.6 show the plausibility maps for the hypotheses „fire“ and „no fire“, respectively. As already discussed, the plausibility represents the grade to which a hypothesis cannot be rejected.

The only evidence which allows for a rejection of the hypothesis „fire“ is given by the distribution of coal seams. However “fire” can only be rejected where coal deposits are absent, that is outside the syncline. Inside the syncline evidence neither for nor

against the presence of a fire can be inferred from presence of coal deposits. Mathematically, plausibility is the remainder after subtracting the belief map for "no fire" from a constant raster with value 1. The plausibility map „fire" therefore constitutes the complement to the belief map „no fire", exhibiting constant high values inside the syncline and zero values outside the outermost coal seam outcrop. Conversely, the plausibility for the hypothesis „no fire" is complementary to the belief map „fire" meaning that high plausibility for „no fire" corresponds to low belief in „fire" and vice versa.

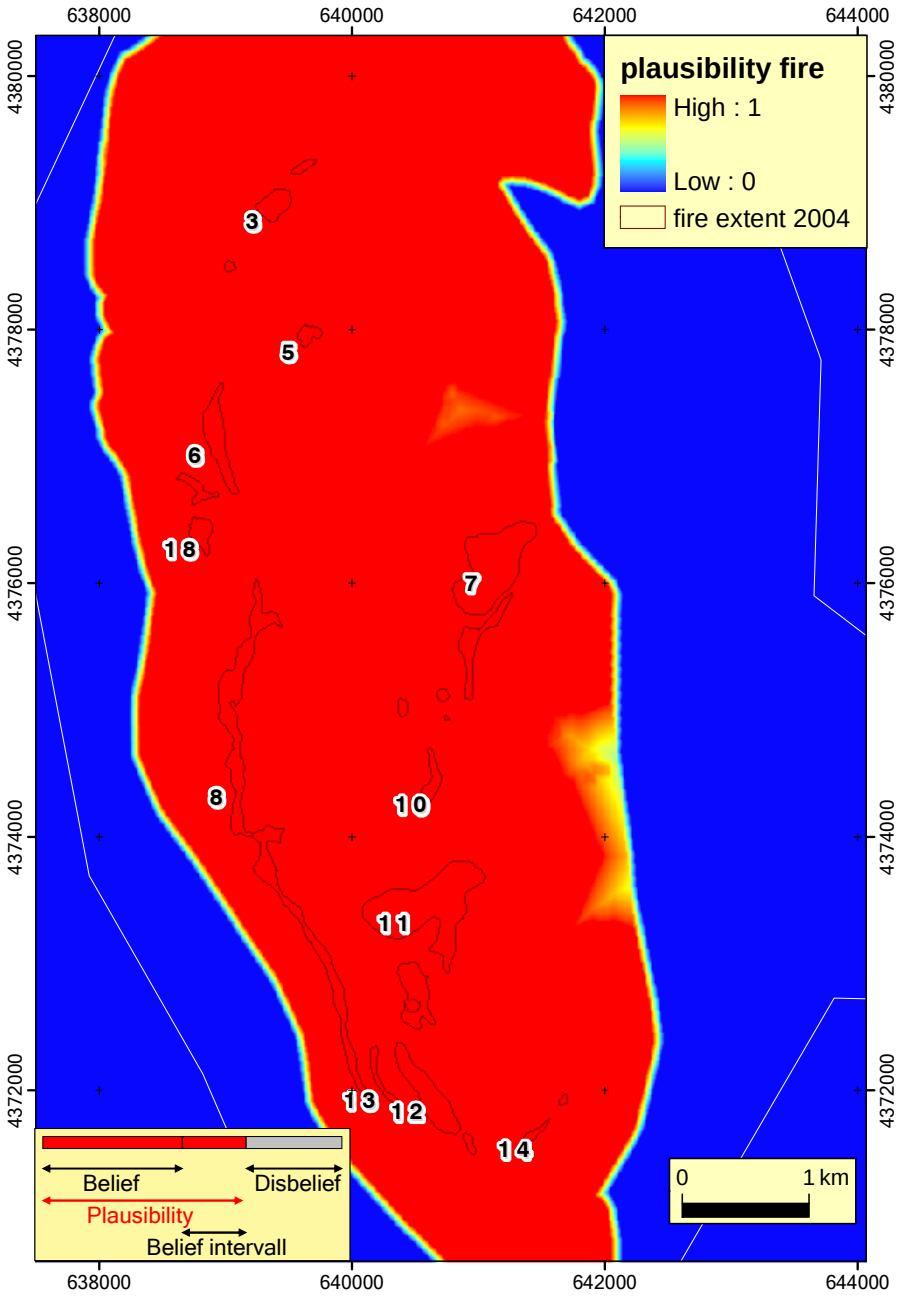

Figure 7.5: Plausibility map generated for the hypothesis „fire"

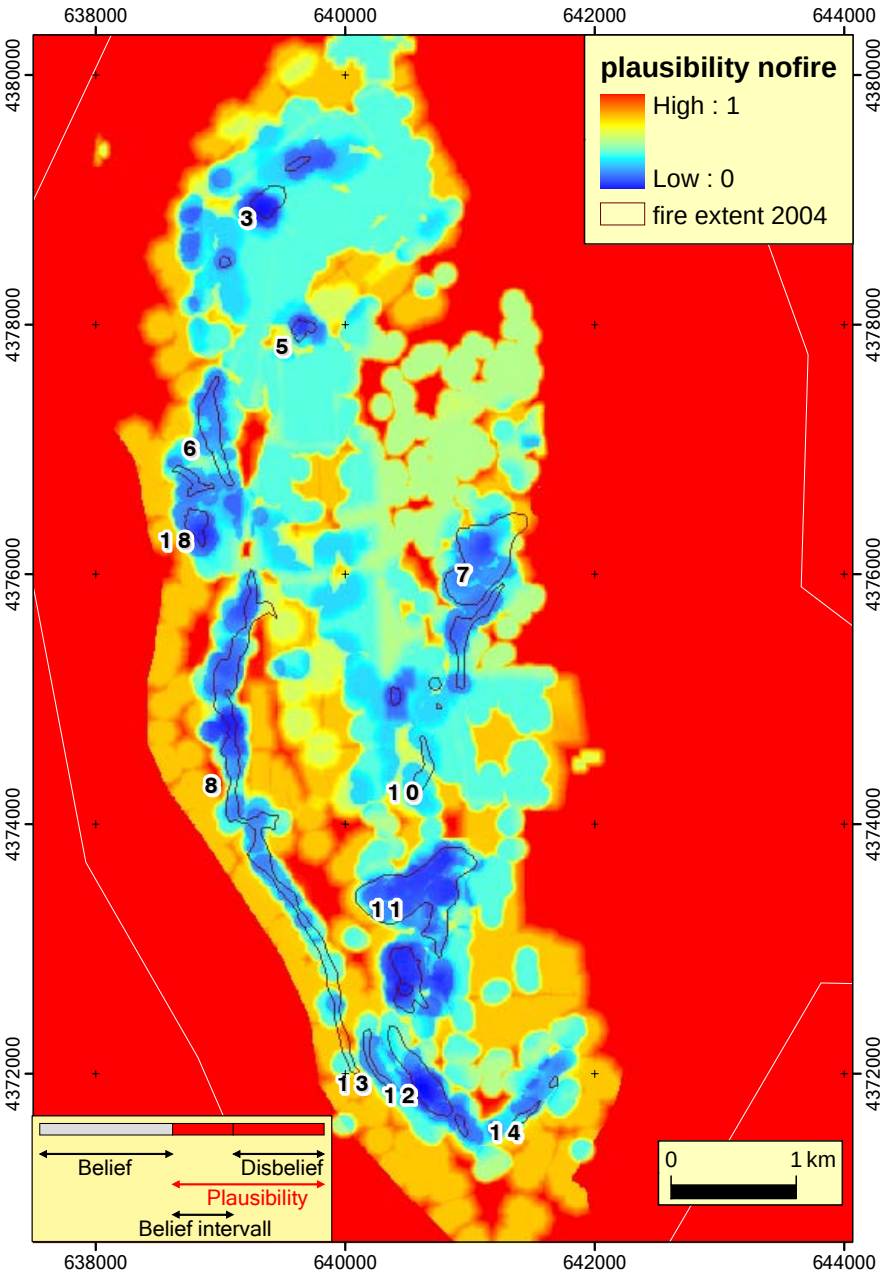

Figure 7.6: Plausibility map generated for the hypothesis „no fire“

7.2.4 Belief interval maps for the hypotheses “fire” and “no fire”

The belief interval maps for both hypotheses are shown in figures 7.7 and 7.8. It is striking that on the belief interval map „fire“, lowest values are found inside as well as outside the syncline. Minima inside the syncline correspond to local maxima on the belief map “fire”. This is due to the fact that uncertainty about the hypothesis „fire“ is zero where strong evidence points to the presence of a fire. Uncertainty about the hypothesis „fire“ also adopts zero values if both, the corresponding belief and

plausibility are zero, which is the case outside the syncline. A zero belief interval outside the outermost seam outcrop indicates the lack of direct evidence for the presence of a fire concomitant with the presence of undoubted evidence for the absence of a fire.

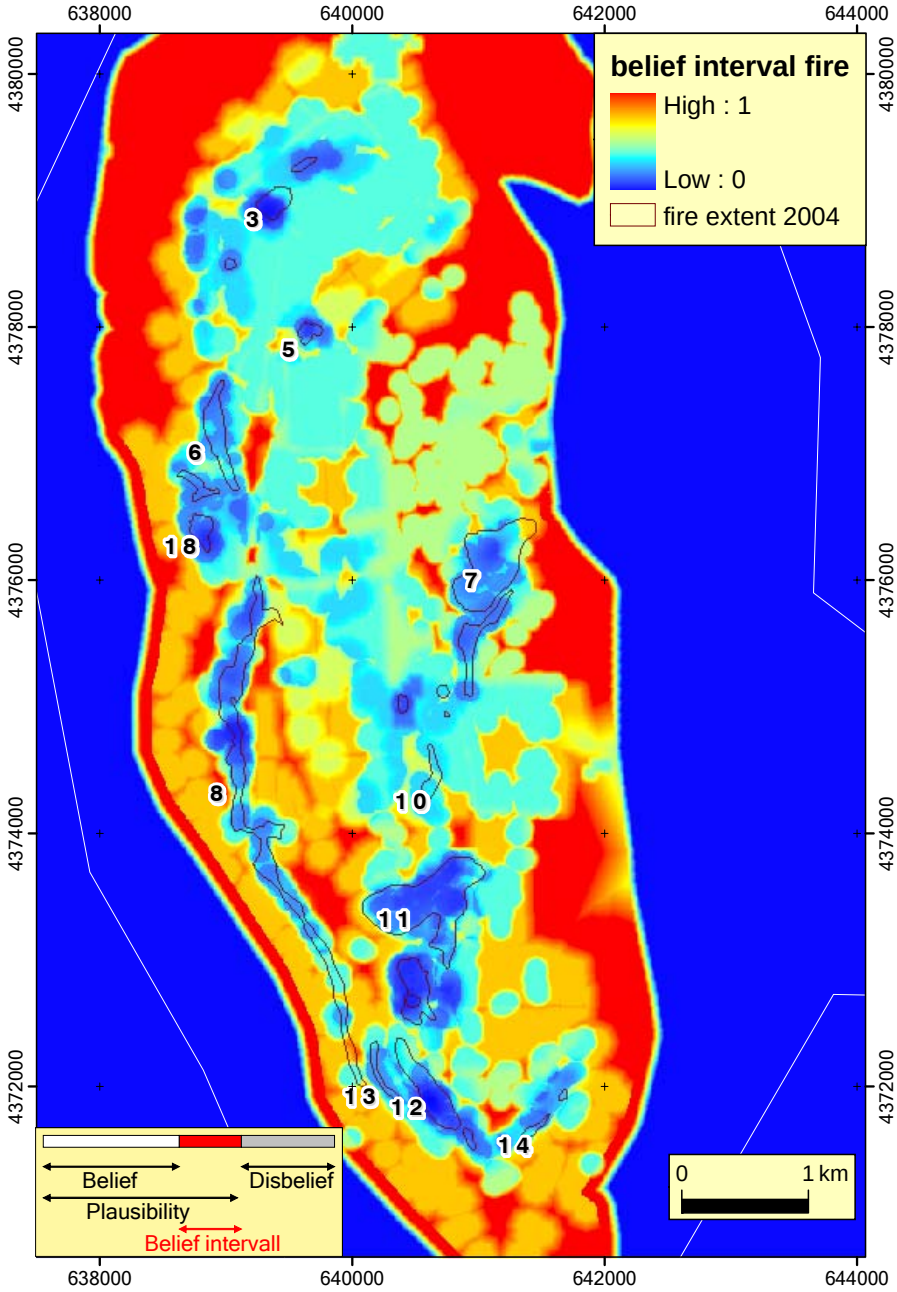

Figure 7.7: Belief interval map generated for the hypothesis „fire“

It is further remarkable that the belief interval map „no fire“ is identical to the one for the hypothesis „fire“. Here, zero uncertainty outside the syncline result from maximum values in the corresponding belief and plausibility maps. Maximum values of belief result from direct evidence through the absence of coal deposits. Maximum

values of plausibility are due to the fact that evidence to reject the hypothesis „no fire“ outside the syncline is zero. In contrast, low uncertainty inside the syncline coincides with strong belief for „fire“. This is comprehensible given that both, the belief and the plausibility for „no fire“ must be low where the presence of a fire is very likely.

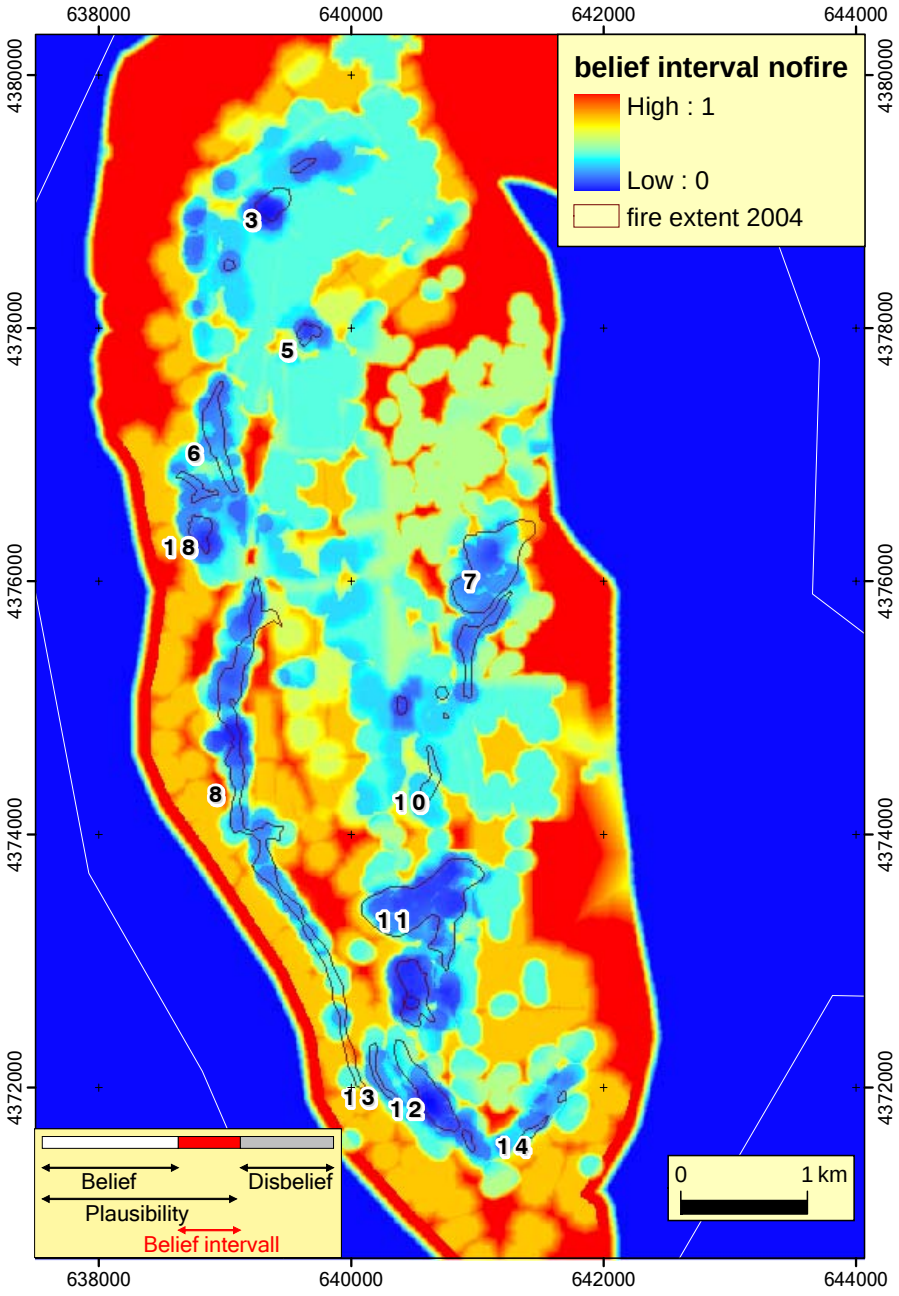

Figure 7.8: Belief interval map generated for the hypothesis „no fire“

7.3 Sensitivity Analysis

To predict the performance of the DS algorithm when applied to transfer areas it is substantial to identify the key indicators for its capability to detect subsurface coal fires. In this context the contribution of indicators with critical availability is of particular interest. For transfer areas, the data base is very likely to be less comprehensive. In particular, field data such as temperature measurements, coal seam distribution and extent of goafs, as well as geological and fire related expert knowledge might not be available. Indeed, a more realistic scenario is to assume that only satellite derived data such as thermal anomalies, cracks, mine activity along with some geological field data (e.g. the range of coal deposits) will be available for fire probability analysis. Focus on the contribution of field temperature measurements as indicator was suggested by an additional reason. Since a considerable number of measurements were made at known fire locations, it was not possible to test the results of the algorithm against data from a truly independent source whenever temperature data were included.

But not only the data base will differ from the one used in this case study, different geological and mining related conditions might also require an adjustment of the geometric constants used in the spatial probability functions. This pertains to the geometric relations between the combustion zone and surface cracks as well as to the maximum depth of coal fires and the sedimentology of coal seams.

In the sensitivity analysis performed within this thesis, the influence of the incorporated data sets was evaluated by means of creating belief maps for different transfer scenarios with varying data input. In doing so, the respective data set under consideration and additionally the field temperature data set were omitted at a time. In addition, test runs with modified probability functions were carried out. Influence on the detection capability of the algorithm was defined based on the degree to which known fire areas are reflected by spatially congruent and distinct belief maxima on the belief map for the hypothesis „fire“. To quantify the influence, difference images were created from the resulting belief maps given full data input and incomplete data input, respectively. The absolute differences were preferred to percentage differences to avoid misleading high percentages resulting from changes at locations with low initial belief values. The maps discussed in the following sections refer to the belief in the hypothesis „fire“.

7.3.1 Transfer scenario: sparse or no field temperature data

To investigate the influence of the temperature data, a random selection was generated comprising 1/8 of the initial measurement points. The free extension Hawth's Analysis Tools for ArcGIS 9.x was used for generating the selections. (download from http://www.spatialecology.com/htools (29.11.05))

Figure 7.9 A shows the belief map as resulting from employment of the randomly selected temperature data points. It is striking that the area of the local belief maxima has decreased distinctively, which results in the extent of these fires being poorly reflected. This is true in particular for fire 8, the lower part of which is not covered. The fire zones 6 a, 7, 10 and 12 in contrast are not represented by distinct maxima at all. The difference map (Figure 7.9 B) shows loss of belief in the vicinity of all fires. Observable belief gains on this map are due to internal effects of the kernel density function. If all temperature data is omitted, changes are even more pronounced (figures 7.9 C and D). Maximum belief values are below one and extensive loss of belief occurs in the range of virtually all known fires. With decreasing maximum probability values separability of the fires from their background is deteriorating significantly. Most of the known fires fall into a wide range zone with moderately enhanced probability, which is interspersed with local maxima resulting from thermal anomalies.

Altogether, field temperature data is a crucial indicator for the detection capability of the algorithm. Without these data, some fires are not reproduced in their full extent or even not detected at all in the study area. Thus, in the related transfer scenario, a considerate number of fires will not be detected. More over, the extent of fires might be underestimated.

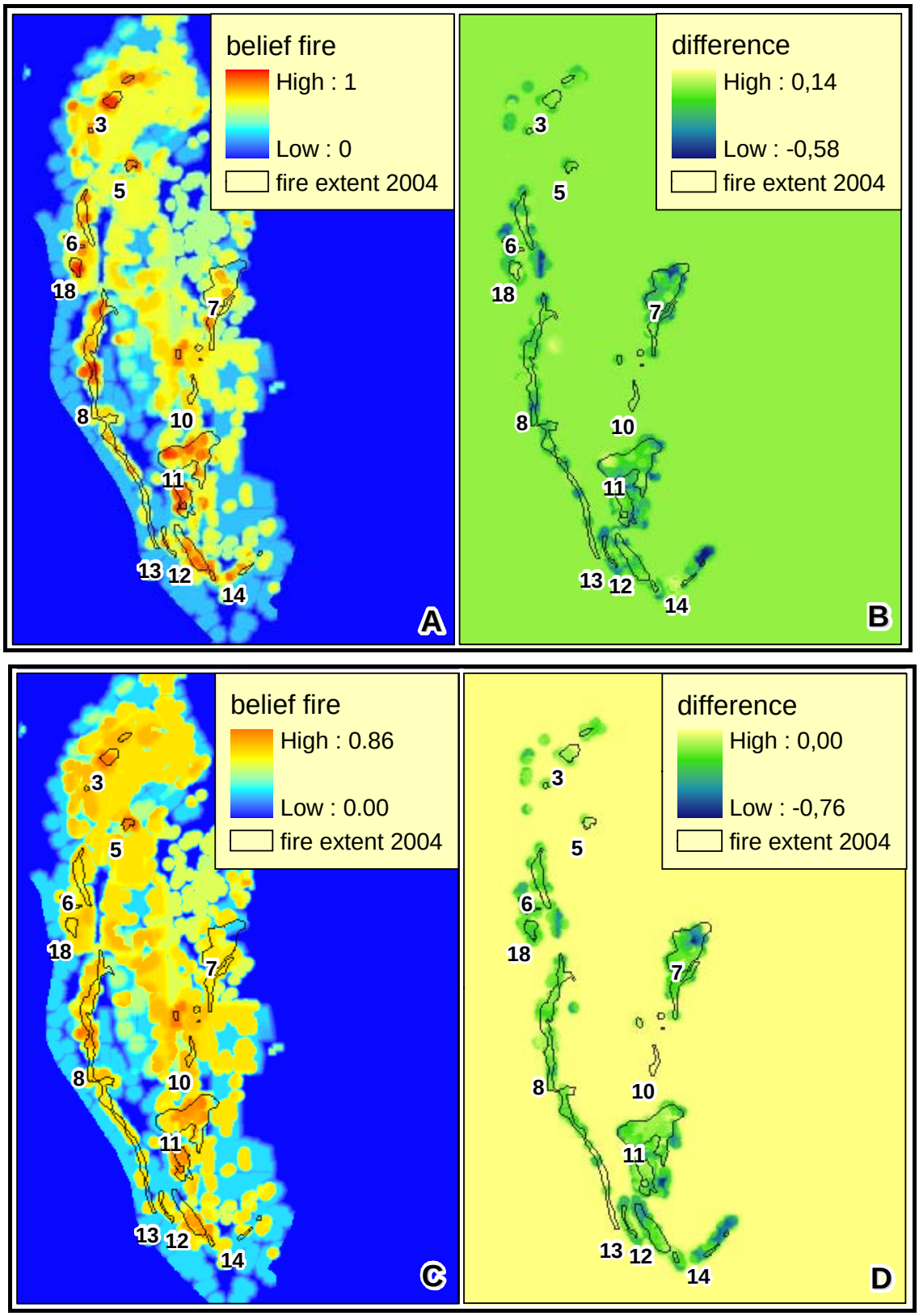

Figure 7.9: Belief maps employing 12.5% of the intial temperature data points (A) and for missing temperature data (C). Difference rasters for the respective belief map and the belief map given full data input (B and D)

7.3.2 Transfer scenario: no LS7 ETM+ thermal anomaly and field temperature data

Figure 7.10 A and B show the belief and difference maps for the hypothesis „fire“ when both, the anomaly data and the temperature data are missing. The known fires are contained within a widespread zone of moderately enhanced probability due to cumulative belief from crack, mine activity and long wall mining data. Although cracks constitute a direct fire indicator, they prove to be rather unspecific with respect to spatial extent. Hence, individual fires are not separated from their background. Looking at the difference map, the combined contribution of the anomaly and temperature data becomes even more evident: the loss of belief in the hypothesis „fire“ is predominantly concentrated on the area of the known fires. It can therefore be concluded that thermal anomalies, apart from the temperature data, constitute the indicator with the highest contribution to the capability of the algorithm to detect fires.

In a transfer scenario with both data sets missing, the algorithm will most probably not be capable to locate existing fires. Belief maps based on this database express fire ignition risk rather than probabilities for existing fires.

7.3.3 Transfer scenario: no crack and field temperature data

The belief map in Figure 7.10 C was created omitting temperature and crack data. It is obvious, that the crack data contributes extensively in the range of medium to high belief. The remaining belief resulting from longwall mining and mine activity data only form a background of weakly enhanced belief. Known fires are reproduced as local belief maxima only where thermal anomalies coincide with the area of these fire. Thus fires 3, 5, 11 and 12 and parts of fire 8 and 10 can still be identified on the belief map, whereas fires 6, 7, 12, 14 and 18 are not detected at all. It is also questionable if the full extent of fire 8 would be discerned during field inspection. Likewise, the difference map (figure 7.10 D) shows that the combined loss of belief through exclusion of crack and temperature data is rather large in area, with some local maxima in the range of the known fire areas.

In summary, cracks are not crucial with respect to fire detection. In a transfer scenario where crack and field temperature data are absent, fire detection hinges on the

thermal anomaly data, which might allow for detection of fires with strong thermal expression at surface.

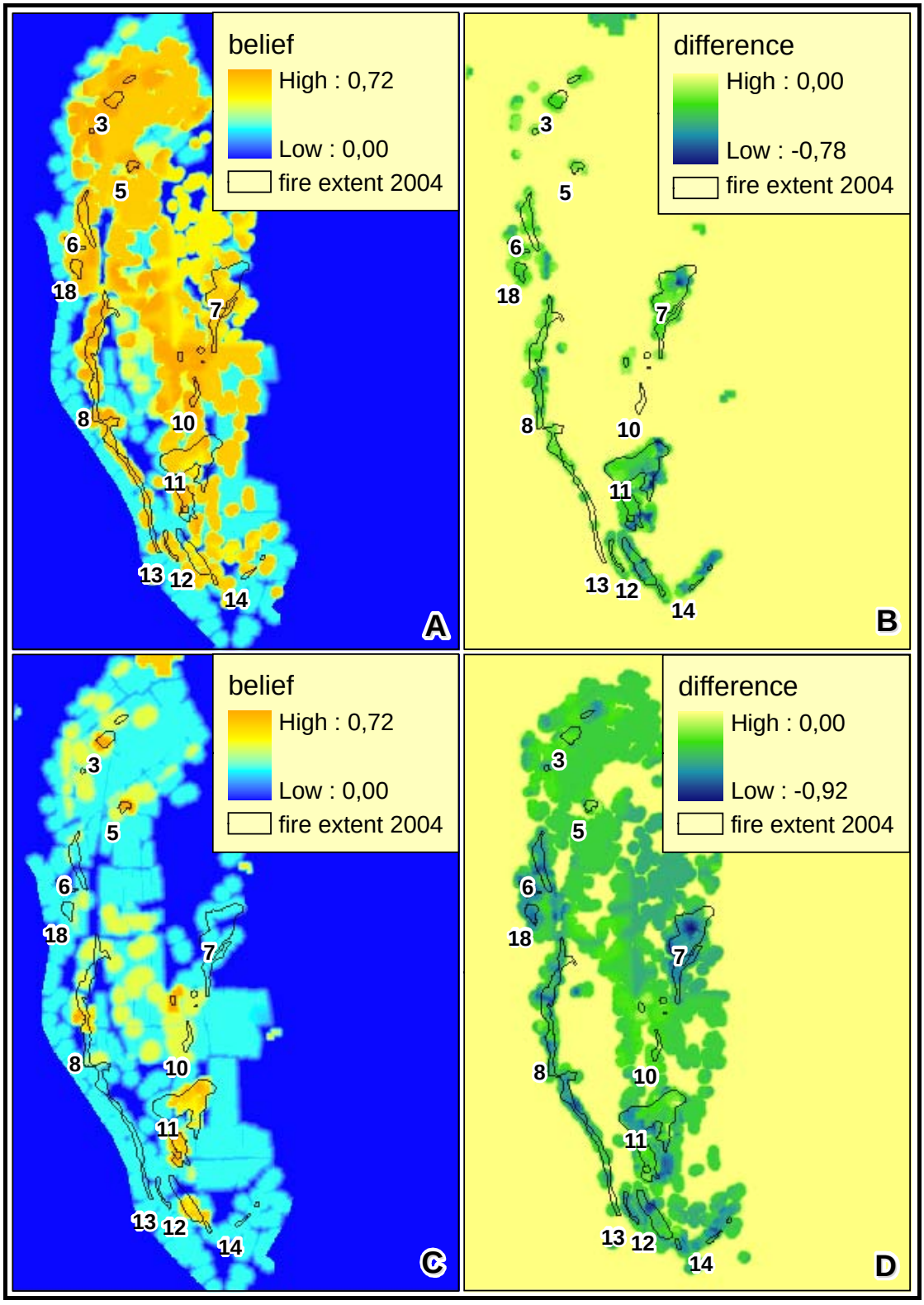

Figure 7.10: Belief maps for missing thermal anomaly and temperature data (A) and for missing crack data plus temperature data (C). Difference rasters for the respective belief map and the belief map given full data input (B and D)

7.3.4 Transfer scenario: no longwall mining or mining activity and field temperature data

The belief maps (figures 7.11 A and C) show that both datasets do not contribute significantly to the fire detection capability of the algorithm. Regardless of which data set is omitted, it is the thermal anomalies that allow for a reproduction of some of the known fire areas, in particular fires 3, 5, 11 and 12. Fires 6, 7, 12, 14 and 18 are not detected and only small portions of fires 8 and 10 are reproduced. Belief loss is predominantly low with maxima (figures 7.11 B and D) due to the lack of temperature data. Again, thermal anomalies account for the detection capability in the underlying transfer scenario implying that fires with weak thermal surface expression might be ignored.

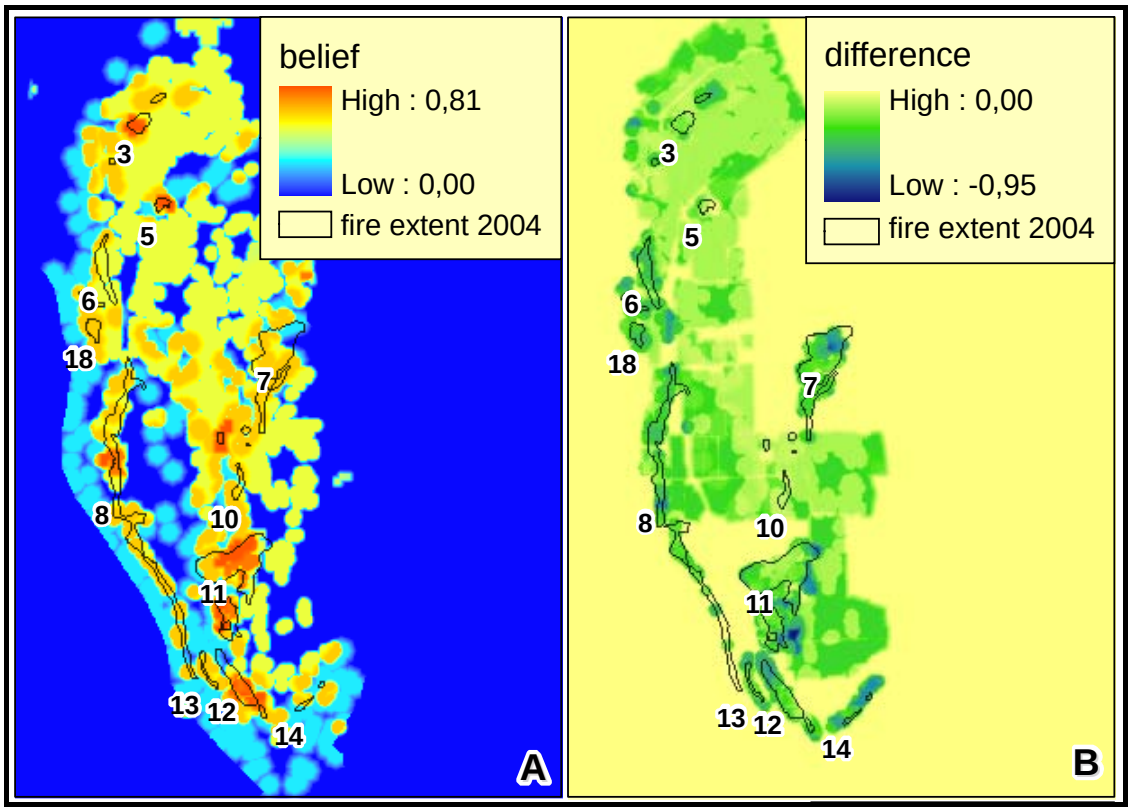

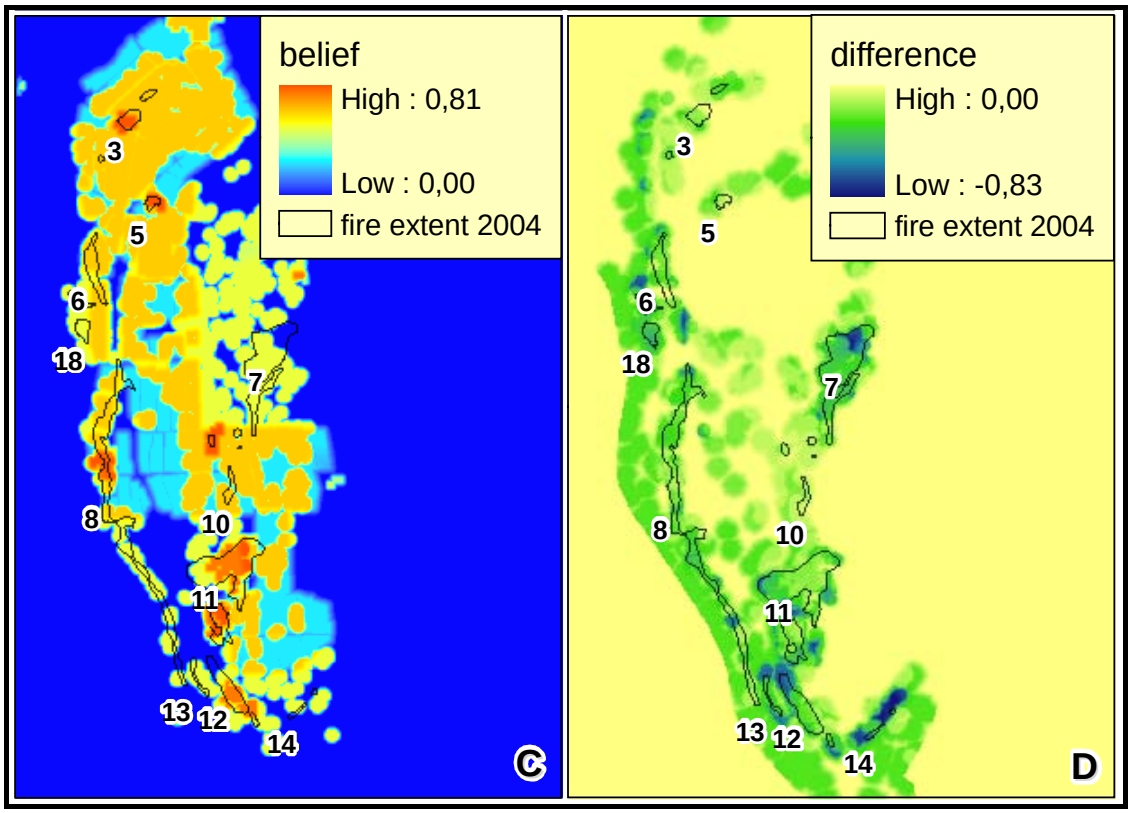

Figure 7.11: Belief maps for missing longwall mining and temperature data (A) and missing mine activity data and temperature data (C). Difference rasters for the respective belief map and the belief map given full data input (B and D)

7.3.5 Transfer scenario: no coal seam and field temperature data

The maps in figures 7.12 A and B were generated without the coal seam distribution and the field temperature data. The belief map „fire“ is not shown, for exclusion of the coal data set doesn't modify the belief in this hypothesis. This is due to the fact that evidence for the hypothesis „fire“ and "no fire" is spatially disjoint. Belief „no fire“ is zero, since coal data constitutes the only evidence for this hypothesis. Consequently, plausibility for the hypothesis „fire“ is one, since the plausibility is constrained by the belief in the counter hypothesis, "no fire". The plausibility map „no fire“ differs from the one given full data input only due to the missing temperature data. Noteworthy differences concern the belief interval maps. Comparing the respective maps for included (figures 7.12 C and D) and omitted (figures 7.12 A and B) coal seam distribution data, it becomes evident that the coal seam data reduces inconclusiveness outside the outermost outcropping coal seam. If evidence from the coal seam distribution is missing the belief interval for both hypotheses equals one in acknowledgement of the fact that evidence for neither of the hypothesis is present outside the syncline.

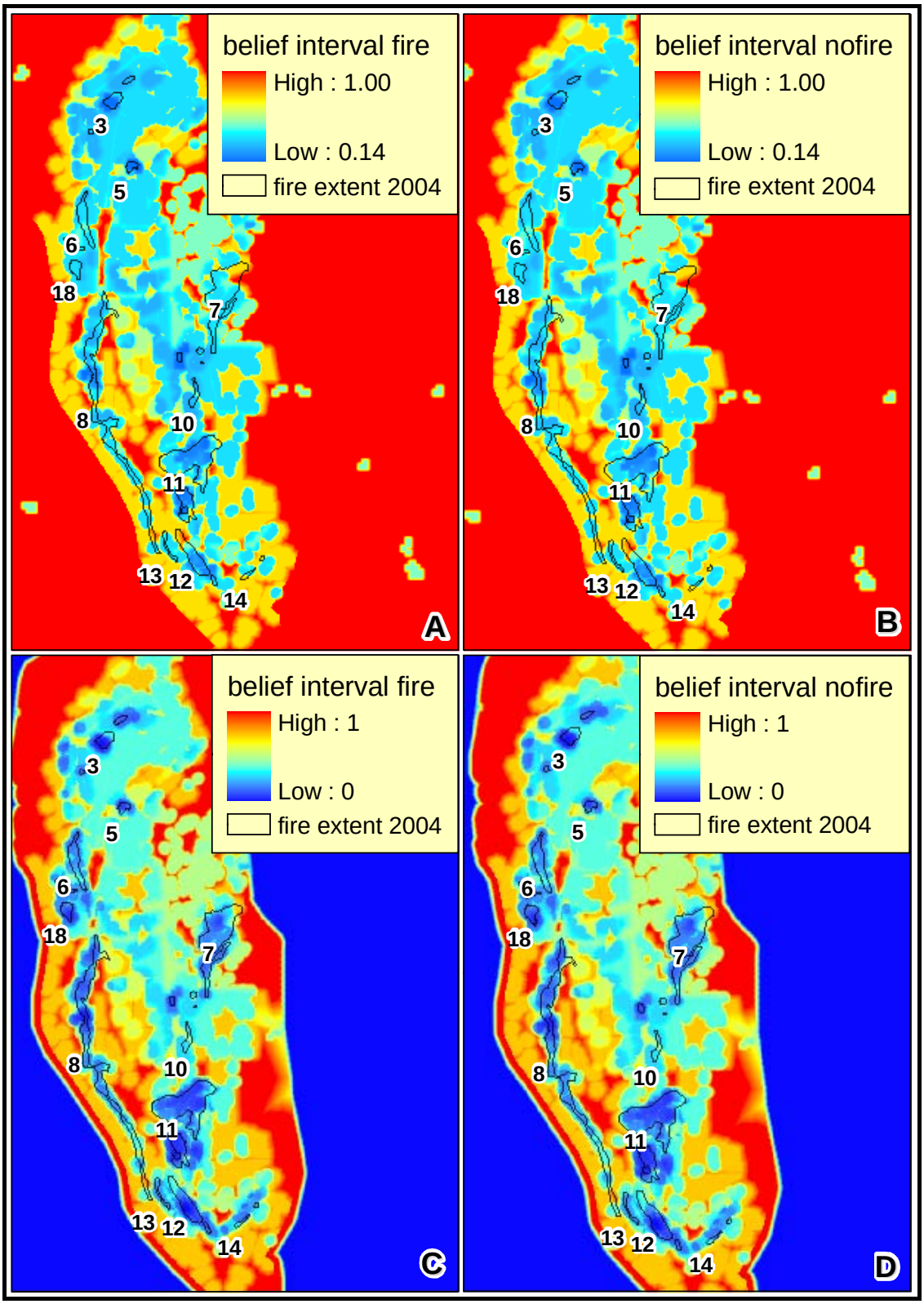

Figure 7.12: Belief interval maps for missing coal seam distribution and temperature data for the hypothesis „fire“ (A) and the hypothesis „no fire“ (B) compared to the corresponding belief interval maps given full data input (C and D)

Of course, conclusions drawn from the study area are not particularly significant for transfer areas, since evidence for and against the hypothesis "fire" might not be spatially disjoint. Incorporation of information on coal deposit distribution in this case will modify belief in the presence of a fire, which will be discussed in the next section.

7.3.6 Transfer scenario: different geometric constants

Figure 7.13 A shows the resulting belief map for the hypothesis „fire" given a maximum fire depth of 75 m (initial value 150 m) and bisected zones of enhanced probability around mining activity and longwall mining features (initial value 100 m). The position of existing fires is rendered by belief maxima, while the extent of the fires, in particular that of fires 6, 7 and 8 is reproduced significantly worse. It can therefore be concluded that variation of the geometric constants has a considerable influence on the capability of the algorithm to estimate fire extents. This implies that although retrieval of the fire extent is limited, localization of fires will not be significantly be impeded in the given transfer scenario.

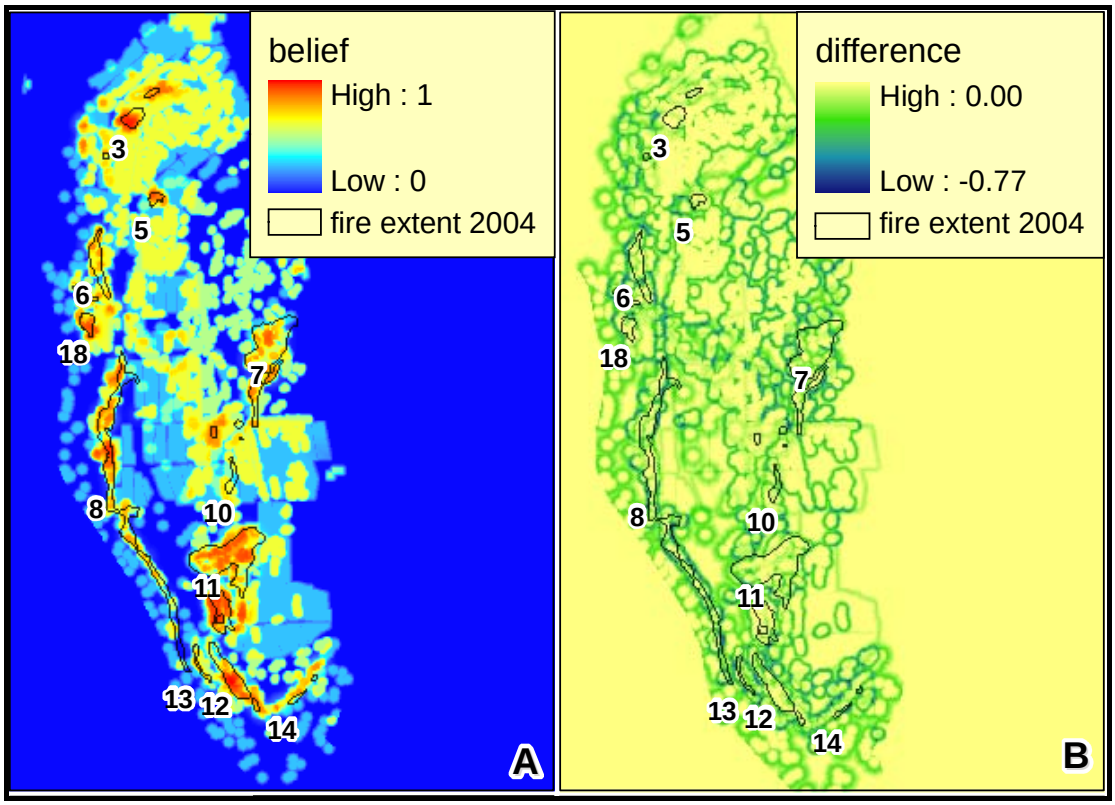

Figure 7.13: Belief map for the hypothesis „fire" under the assumption of a maximum fire depth of 75 m (A) and difference to the initial belief map when a maximum fire depth of 150 m is assumed (B).

Figure 7.14 A shows the belief map when dip angles of the seams steeper than 20° are assumed. This implies a reduction of the zero probability and transition zones for the hypothesis "no fire" to ~ 400 m (initial value 1700 m) around the coal seam outcrops. Conversely, the zone with zero belief for the hypothesis "fire" extends further into the syncline. Conflicting evidence now occurs inside the syncline as indicated by the blue (zero value) areas in figure 7.14 B. Belief "fire" less than one is in a figurative way absorbed by coinciding probability of 1 for the absence of a fire (see also table 7.1). If probability for the absence of a fire is not zero, the belief in the hypothesis "fire" is reduced accordingly. In the transfer scenario the coal data is likely to differentiate belief distribution by locally weakening belief in the hypothesis "fire" and to confine the area to be searched for fires.

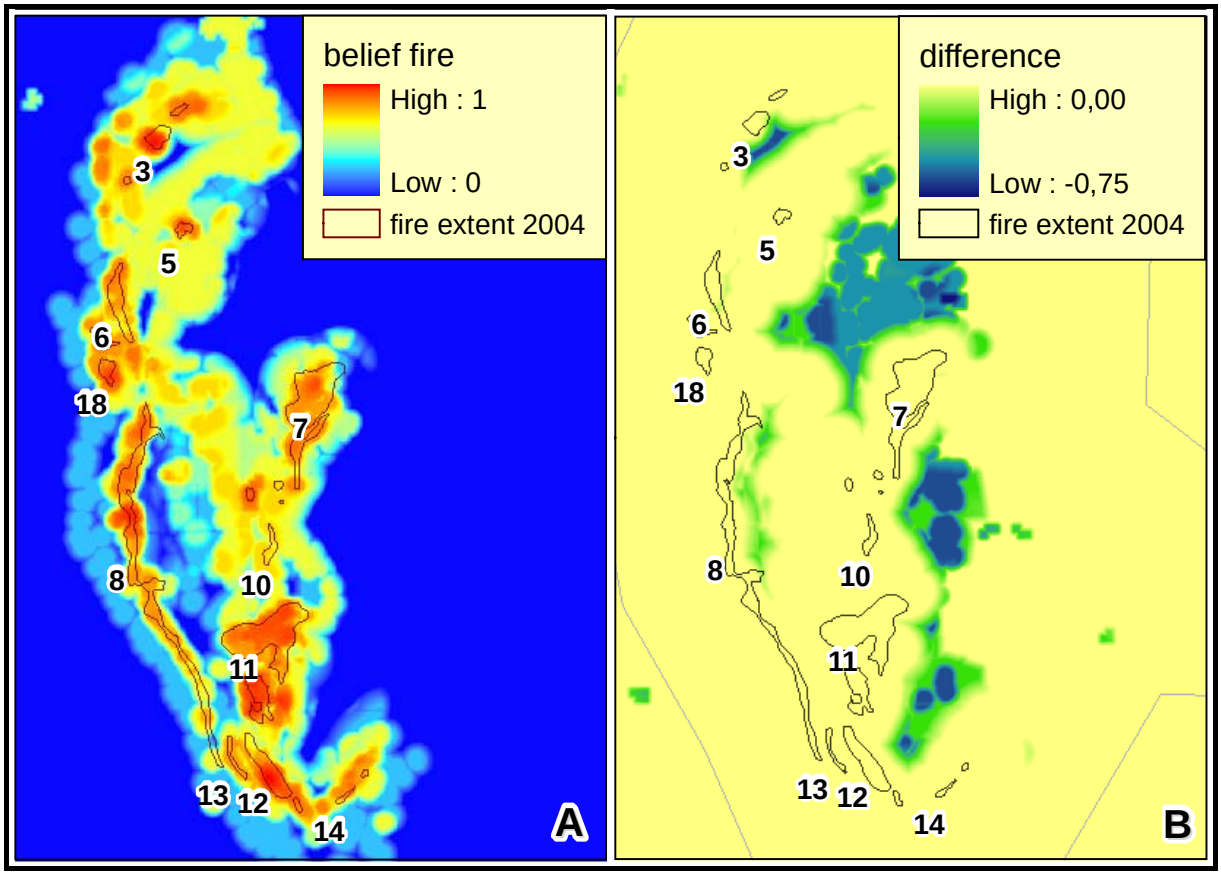

Figure 7.14: Belief map for the hypothesis „fire" under the assumption of a maximum fire depth of 150 m and a shallowest dip angle of ~ 20° (A) and difference to the initial belief map (B).

7.3.7 Most probable transfer scenario

Figure 7.15 shows the resulting belief map for missing field temperature and longwall mining data. This was argued to be the most probable transfer scenario. Fires 3, 5, 11, 12 and

small parts of fires 8 and 10 are detected, whereas fires 6 and 14 are not detected at all. Fires 7, 10, 13, 18 and a large part of fire 8 coincide with zones of moderately enhanced belief, which yet show a spread far beyond the area of these fires. The detection capability of the algorithm hinges on the combined evidence from thermal anomalies and cracks. It can therefore be expected that fires expressed through both, large area and/or intense thermal anomalies and surface cracks will unambiguously be detected. Detectability of fires characterised by one of the two indicators will depend on the abundance of non fire causes for the respective indicator. In areas with sparse settlement and limited subsurface mining activity belief maxima through one of these indicators might be pronounced enough to qualify as priority area for further investigation. Even if anomalies and cracks do not allow for detection of existing fires belief maps can serve to identify areas with enhanced fire risk. Anyway, interpretation of belief maps and subsequent derivation of action plans will always be subject to the individual objectives of the interpreter. Last but not least the financial and technical resources will be a key factor in this context.

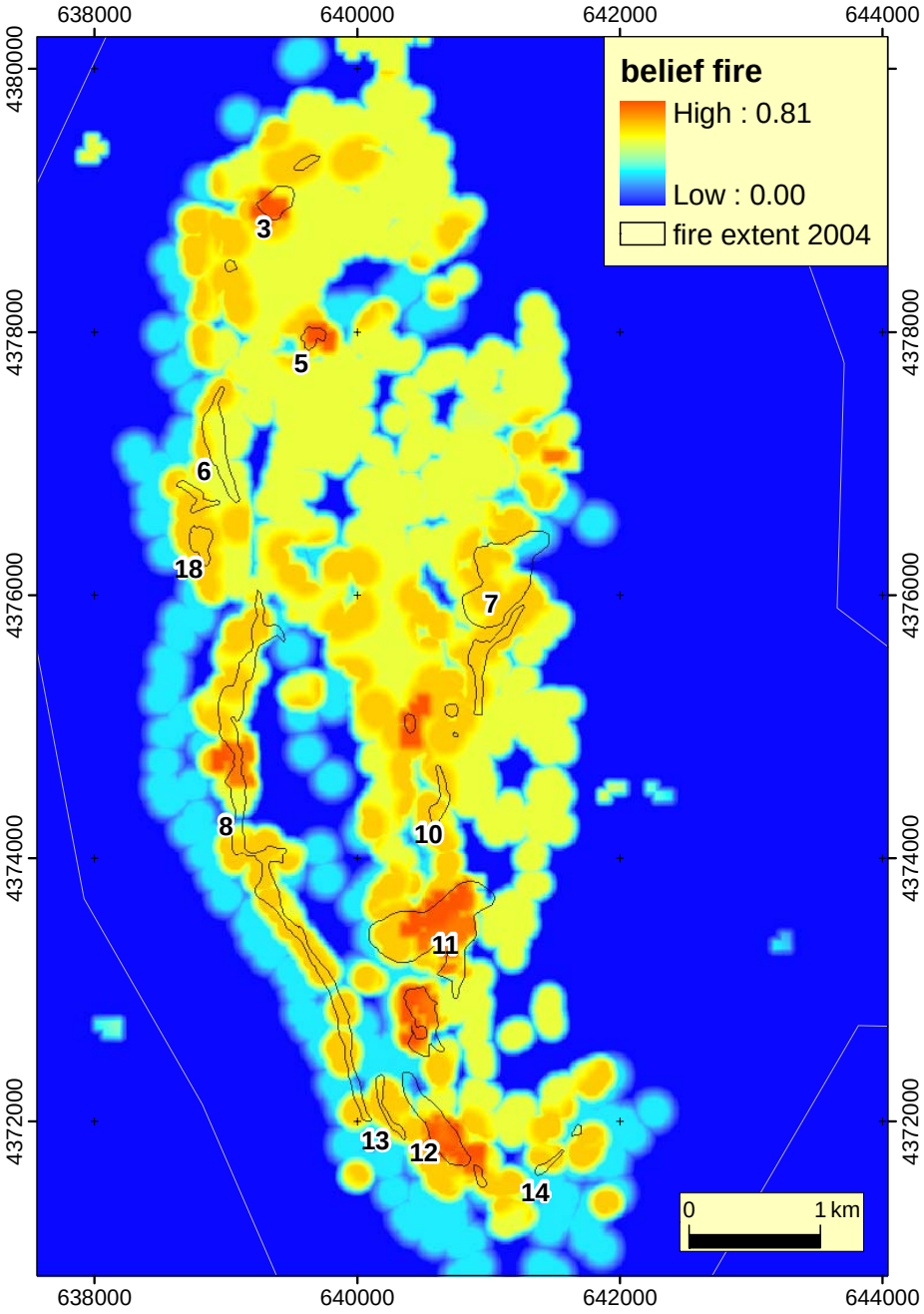

Figure 7.15: Belief map for the most probable transfer scenario

7.4 Evaluation with respect to the goals defined

It has been discussed that uncertainty is inherent in the available data and this uncertainty can effectively been handled by DST. Probabilities used as basic information level in DST have proven to be a suitable parameter to abstract and standardize fire relevant information delivered by the different indicators. In addition, the current chapter showed that the logic of summing the evidence according to DST can effectively be implemented in a GIS based framework. Therefore, the main goals on the conceptual level were achieved.

With respect to the goals on the implementation level it can be summed that the belief map for the hypothesis “fire” combining all available evidence reproduces the known fire areas significantly better than the isolated probability maps. Assuming that there was no prior information, the existing fires in the study area could very effectively be pinpointed in the field using the belief map as a guide. Therefore, The belief map for the hypothesis „no fire“ supports these activities in that search for fire sources can be focused on a smaller area. The plausibility maps here do not yield utilizable visual information, since the evidence for both hypotheses is spatially disjoint. Important conclusions can also be drawn from the belief interval maps. As information gain by additional evidence is highest in places where belief and plausibility for one hypothesis diverge most, these will be the areas of interest when further investigation reveals new evidence. Thus, belief-, plausibility- and belief interval maps are a suitable visualization solution promoting

- intuitive information on probable fire locations and fire risk areas even of geographically untrained viewers
- and hands on orientation for fire extinguishing activities in the field.

Ensuring transferability of the DS analysis tool was a further goal specified in section 1.3. Extent of the available data and the geometry of the probability functions are the parameters likely to differ in the transfer case. It was shown that in the most probable transfer scenario with respect to the available data base the tool can be expected to detect fires with strong thermal expression at surface and in addition to provide information on fire risk throughout the study area. Varying geometric constants will in the first row pertain to the crack and the coal seam distribution data which might significantly modify their role and contribution in belief modelling for the hypothesis “fire”. In acknowledgement of both moments of variance the application implementing the algorithm allows for choice of input data sets as well as geometric constants which can be adjusted to the situation in the respective transfer area.

7.5 Summary

Apart from the field temperature data, known fire areas are not reproduced by the probability maps based on single indicator data. In contrast, local maxima in the belief maps for the hypothesis „fire“, which are based on combined evidence from six selected indicators reproduce location and extent of the known fire areas very well. Belief in the hypothesis „no

fire“ is high where coal deposits are absent. This map may be used to confine the search area for fires. The plausibility maps are complementary to the respective belief maps for the counter hypothesis. They do not yield additional information. The belief interval maps are identical for both hypotheses showing low values where belief in either of the hypotheses is strong. They give a hint where information gain can be expected to be highest when new evidence emerges.

The performance of the algorithm in transfer scenarios with different available data bases and geometry of the probability functions was investigated. In doing so, the field temperature data were identified to be the most important contributor to detection capability. Thermal anomalies allow for a reproduction of at least part of the known fire areas, although their extent is not accurately reflected. The remainder of the evidence supporting the hypothesis „fire“ doesn’t allow for a separation of fires from the background. The coal seam distribution data will influence the belief in the presence of a fire, if evidence for the two hypotheses is spatially conjunct. Bisection of the maximum fire depth results in narrower zones of enhanced probability. Fires are still pinpointed but their extent tends to be underestimated. Under a realistic scenario for the available data base, which will predominantly consist of data derived from earth observation, the capability of the algorithm in transfer areas to detect fires is likely to be limited. However, belief maps can be employed to estimate fire risk.

8. Conclusions and recommendations for further research

Dempster-Shafer theory of evidence has proven to be a suitable approach to estimate probability for subsurface coal fires derived from multiple geo related indicators. Inherent uncertainty in the relationship of the evidence and the decision alternatives - presence or absence of a fire - can be modelled effectively by Dempster-Shafer type belief functions.

Given the data base available for the study area, virtually all existing subsurface coal fires can be detected with good accuracy by the DS-based algorithm developed in this thesis. The generated belief maps reproduce location and extent of the fires. For potential transfer areas the availability of field temperature and thermal anomaly data will be a key factor determining fire detection capability of the algorithm. Both data sets were found to contribute the bulk to coal fire detection in the study area. In a realistic transfer scenario where predominantly remote sensing derived data are available, a lower performance of the algorithm can therefore be expected. Likewise, the choice of the geometry of the probability distribution has proved to influence fire detection capability. Expert knowledge used to determine probability functions is area specific and has to be adjusted to the specific situation in the transfer area.

One focus for further research therefore is to apply the algorithm to a transfer area based on a reduced database and employing modified geometry of probability distributions. The results should then be verified by means of field inspection or, if available, by comparison with known fire locations. In addition, future research has to prove if new evidence can compensate for the lack of precise field data. Ongoing research at Bundesanstalt für Geowissenschaften und Rohstoffe (BGR) (SCHAUMANN, 2005 PERS. COMM.) on geophysical signatures of coal fires seems promising in this context. Field experiments in the Wuda area showed that sub surface fires can be correlated with high sub surface conductivities. Further research is on the way studying the possible relationship to the magnetic properties of the rock. Both parameters lend themselves to airborne observation by plane or helicopter, which implies that they might constitute an additional high resolution indicator with coverage in the local to regional range.

Identification of fire zones in the study area was based on visual interpretation of the belief maps. Visual separability of belief maxima on the other hand depends on the display modus chosen and is subject to individual perception. In an operational use of the algorithm, more reliable and comprehensible separation criteria are desirable. Hence, a further research topic is to develop such criteria. One quantitative approach could be the generation of

additional threshold maps supportive to the belief maps. The threshold value could be derived from statistical analysis of the belief values representing known fire areas.

9. Bibliography

BONHAM-CARTER, G. F., AGTERBERG, F. P., AND WRIGHT, D. F. (1988): Integration ofgeological datasets for gold exploration in Nova Scotia. Photogrammetic Engineering and Remote Sensing, 54, 1585–1592.

BONHAM-CARTER, G.F., AGTERBERG, F.P. AND WRIGHT, D.F., (1989): Weights of evidence modelling: a new approach to mapping mineral potential. In: Agterberg, F.P., Bonham-Carter, G.F. (Eds.), Statistical Applications in the Earth Sciences. Geological Survey ofCanada, Paper 89-9, 171– 183.

BP (2005): Statistical Review of World Energy full report; Energy in Focus. Technical report, British Petroleum, London.
(http://www.bp.com/liveassets/bp_internet/globalbp/globalbp_uk_english/publications/energy_reviews_2005/STAGING/local_assets/downloads/pdf/statistical_review_of_world_energy_full_report_2005.pdf)(10.2.2006)

CARRANZA E. J. M., HALE, M. (2002): Evidential belief functions for data-driven geologically constrained mapping of gold potential, Baguio district, Philippines.
Ore Geology Reviews 22, 117–132.

CHUNG, C.F., FABBRI, A.G. (1993): The representation of geoscience information for data integration. Nonrenewable Resources 2 (2), 123 – 139.

CORGNE S., HUBERT-MOY L., DEZERT J., MERCIER G. (2001): Land cover change prediction with a new theory of plausible and paradoxical reasoning.

CUZZOLIN, F. (2004): Geometry of Dempster's Rule of Combination. IEEE Transactions on Systems, Man, And Cybernetics – Part B Cybernetics, Vol. 34, No. 2. 961 – 977.

DEMPSTER, A.P. (1967): Upper and lower probabilities induced by a multivalued mapping. Annals of Mathematical Statistics 38, 325– 339.

DEZERT J., SMARANDACHE F. (2003): On the generation of hyper-powersets for the DSmT. Proceedings of the6th International Conference on Information Fusion, Cairns, Australia, July 8-11.

DUBOIS, D. PRADE, H. (1988): Representation and combination of uncertainty with belief functions and possibility measures, Comput. Intelligence 4 244–264.

EASTMAN, J. R. (2003): Idrisi Manual Version 14.00. Worcester.

GIELISCH, H. (2004): Geology of the Helan Shan – Field Report.

GUAN, J. W., BELL, D. A. (1991): Evidence Theory and its applications. Volume 1. In: Banerji R.B., Kobayashi, H., Montanari, U., Nivat, M. (Eds.): Studies in computer science and artificial intelligence 7. Elsevier Science Publishers B.V., Amsterdam.

HUBERT-MOY, L., CORGNE, S., MERCIER, G., SOLAIMAN, B. (2002): Land Use and Land Cover Change Prediction with the Theory of Evidence : A Case Study in an Intensive Agricultural Region of France.

JØSANG, A. (2002): The consensus operator for combining beliefs.
Artificial Intelligence 141 (2002) 157–170.

KÜNZER, C. (2005): Demarcating coal fire risk areas based on spectral test sequences and partial unmixing using multi sensor remote sensing data. Dissertation at Vienna University of Technology, Vienna.

KUENZER, C., ZHANG, J., TETZLAFF, A., VOIGT, S., VAN DIJK, P., WAGNER, W. & MEHL, H.: Uncontrolled coal fires and their environmental impacts: Investigating two arid mining environments in north-central China. In review at: Applied Geograph

LEE, S. AND CHOI, J. (2004): Landslide susceptibility mapping using GIS and the weight-of evidence model. INT. J. GEOGRAPHICAL INFORMATION SCIENCE
VOL. 18, NO. 8, 789 – 814.

LITSCHKE, T. (2005): Detailed Mapping of Coal Fire Sites in Combination with In-Situ Flux Measurements of Combustion-Gases to Estimate Gas Flow Balance and Fire Development (Wuda Coal Field, Inner Mongolia Autonomous Region).
Masters thesis at University of Duisburg Essen.
LORUP, E. (1999): Belief modelling with Arcview GIS.
http://gis.esri.com/library/userconf/proc99/proceed/papers/pap295/p295.htm
(21.11.2005)

MALCZEWSKI, J., (1999): GIS and Multicriteria Decision Analysis. John Wiley and Sons, New York.

ROSEMA, A., GUAN, H., VELD, H., VEKERDY, Z., TEN KATEN, A.M., PRAKASH, A. (1999): Manual of Coal Fire Detection and Monitoring. Netherland Institute of Applied Geosciences Report NITG 99-221-C.

SAHOO, N.R. JOTHIMANI, P. TRIPATHY, G.K. (2001): Multi-criteria analysis in GIS environment for natural resource development - a case study on gold exploration.
http://www.gisdevelopment.NET/application/geology/mineral/geom0002.htm
(17.02.2006)

SHAFER, G. (1976): A mathematical theory of evidence. Princeton University Press, Princeton, New Jersey.

SMETS, P. (1994): What is Dempster-Shafer`s model? In: Yager, R. R., Kazprzyk, J., Fedrizzi, M. (Eds.): Advances in Dempster-Shafer Theorie of Evidence Wiley, New York, 5 – 34.

TANGESTANI, M., H., MOORE, F. (2002): The use of Dempster-Shafer model and GIS in integration of geoscientific data for porphyry copper potential mapping, north of Shahr-e-Babak, Iran. International Journal of Applied Earth Observation and Geoinformation 4, 65 – 74.

UNITED MINE WORKERS OF AMERICA (2005)
http://www.umwa.org/mining/lwmine.shtml (20.2.2006)

VAN GENDEREN J.L., GUAN, H. (1997): Environmental monitoring of spontaneous combustion in the north China coalfields. Enschede, Netherlands.
WALKER, S. (1999): Uncontrolled fires in coal and coal wastes. IEA Coal Research, London UK.

YAGER, R.R. (2004): On the determination of strength of belief in decision support under uncertainty—Part II:fusing strengths of belief. Fuzzy Sets and Systems 142, 129 – 142.

ZADEH, L., A. (1984): Review of books: a mathematical theory of evidence. The AI Magazine 5 (3), 81–83.

ZHANG, J. (2004): Spatial and statistical analysis of thermal satelitte imagery for extraction of coal fire related anomalies. Dissertation at Vienna University of Technology.

ZHANG, X. (1998): Coal fires in Northwest China. Detection, Monitoring and Prediction using Remote Sensing Data. Enschede, Netherlands

Appendix

A.1 Manual for Dempster-Shafer anlysis tool

Objective/Purpose

Performing Dempster-Shafer belief modelling on specified input data sets. Generation of belief, plausibility and belief interval raster maps to model and visualize coal fire probability.

Platform specification

The application has been tested on Microsoft Windows XP™ operating system with ArcGIS 9.1. Additional requirements are Service Pack 2 for Windows XP as well as the Microsoft .NET framework 2.0 installed on the machine.

Development environment

Visual Basic 2005 Express Edition and ArcObjects 9.1 distributed as executable.

Description of auxiliary files and output files

The files listed below are generated and stored in the working directory

- EucD*VB = distance raster for the respective feature data set
- *ProbVB = probability raster for the respective feature data set
- Ker200VB, KerNormVB, TempProbVB = intermediate results from the kernel density function used to generate the probability map from temperature data
- Aggr*SupFire = the results from combining the different belief masses for the hypothesis fire

The final results are

- FinBel(No)Fire = final belief in the hypothesis (no)fire
- Plaus(No)Fire = plausibility for the hypothesis (no)fire
- Inter(No)Fire = belief interval for the hypothesis (no)fire

Table A1: List of functions based on map algebra

Function	Purpose	Syntax	Result
Single Output Map Algebra	Standardization of the Euclidean distance raster generated from the respective data set	(eucdist_cra < 75) * 0.5 + ((eucdist_cra >= 75) AND (eucdist_cra < 150)) * (eucdist_cra - 150) / (0 - 150) + (eucdist_cra >= 150) * 0	Fire probability map derived from crack data
		(eucdist_temp < 75) * 0.75 + ((eucdist_temp >= 75) AND (eucdist_temp < 150)) * (eucdist_temp - 150) / (0 - 100) + (eucdist_cra >= 150) * 0	Fire probability map derived from field temperature measurements
		CON([eucdist_ano] == 0, 0.5, ([eucdist_ano] > 0 AND [eucdist_ano] <= 60) * (([eucdist_ano] - 60) / (0 - 120)) + (([eucdist_ano] > 60) * 0))	Fire probability map derived from thermal anomalies in LS7 band 6 data
		CON ([eucdist_long] == 0, 0.25, ([eucdist_long] > 0 AND [eucdist_long] <= 100) * (([eucdist_long] - 100) / (0 - 400)) + (([eucdist_long] > 100) * 0))	Fire probability map derived from distribution of longwall mining activity
		(costdis_act <= 100) * 0.25 + ((costdis_act > 100) AND (costdis_act <= 200)) * ((costdis_act - 200) / (0 - 400)) + (costdis_act > 200) * 0	Fire probability map derived from distribution of surface mining related features
		(CostDis_Coal <= 850) * 0 + ((CostDis_Coal > 850) AND (CostDis_Coal <= 1700)) * ((CostDis_Coal - 850) / 850) + (CostDis_Coal > 1700) * 1	Fire probability map derived from distribution of coal deposits

Table A1 continued: List of functions based on map algebra

Function	Purpose	Syntax	Result
	Orthogonal summation of probabilities supporting "fire"	probability map A * probability map B + (1 - probability map B) * probability map A + (1 - probability map A) * probability map B (prototype syntax)	Aggregated probability map "fire"
	Orthogonal summation of aggregated probabilities "fire"and "no fire"	(1 – coal probability map) * final probability map fire / (1 – coal probability map * final probability map fire)	Belief map "fire"
		(1 – final probability map fire) * coal probability map / (1 – coal probability map * final probability map fire)	Belief map "no fire"
	Generation of plausibility and belief interval maps	1 – belief_nofire	Plausibility map "fire"
		1 – belief_fire	Plausibility map "no fire"
		Plausibility_fire – belief_fire	Belief interval map "fire"
		Plausibility_nofire – belief_nofire	Belief interval map "no fire"